Surface Wave–Turbulence Interactions: Scaling $\epsilon(z)$ near the Sea Surface

A. ANIS AND J. N. MOUM

College of Oceanic and Atmospheric Sciences, Oregon State University, Corvallis, Oregon

(Manuscript received 10 May 1994, in final form 12 December 1994)

ABSTRACT

A freely rising profiler was used to collect vertical microstructure profiles in the upper oceanic boundary layer under various atmospheric and sea conditions. Near the sea surface, the rate of viscous dissipation of turbulence kinetic energy, ϵ, exhibited a range of behaviors under different forcing conditions. Sometimes, ϵ was closely balanced by the wind stress production of turbulence kinetic energy. At other times, ϵ was greatly enhanced relative to wind stress production and exhibited an exponential depth decay. In these instances, simple scaling laws predicted for turbulence near a solid surface severely underestimate turbulent mixing near the ocean surface.

Plausible explanations for enhanced $\epsilon(z)$ near the sea surface will have to address the effects of wave–turbulence interactions. The authors propose two different mechanisms to explain the behavior of ϵ near the surface, leading to two scaling schemes. The first mechanism requires high levels of turbulence kinetic energy, created by wave breaking at the surface, to be transported downward away from the surface by the motion of the swell. This transport is then locally balanced by ϵ. The second mechanism requires a rotational wave field and significant wave stresses that balance the turbulence Reynolds stresses. Energy drawn from the wave field to the mean flow, via the wave stresses, is in turn drawn from the mean flow by the turbulence production term, which is balanced by ϵ.

1. Introduction

The ocean boundary layer (OBL) is defined as that part of the ocean directly influenced by surface forcing such as heat flux, wind stress, and surface waves. As a result, the OBL responds directly to changes in surface forcing with timescales on the order of diurnal timescales (e.g., the diurnal heating/cooling cycle) or shorter scales. The upper boundary of the OBL is the ocean's surface, while the lower boundary is often defined by the top of the seasonal thermocline.

In spite of the crucial role of the OBL in atmosphere–ocean dynamics our understanding of the physics in the OBL is rudimentary at best. In a recent review of air–sea interaction, Donelan (1990) concluded that the largest gap in our knowledge of air–sea interaction is in the relationship between the OBL and surface waves. A major obstacle to the understanding of processes in the OBL is the scarcity of accurate measurements. They are difficult to accomplish due to the need for a stable platform from which to make the observations and due to the harsh environment in which the sensors need to operate. Moreover, the analysis is usually complicated as one has to evaluate independently the motions due to the mean flow, waves, and turbulence.

Numerical models, which predict the response of the ocean to different atmospheric forcing conditions, are crucially dependent on accurate parameterizations of momentum, heat, and gas exchange between the atmosphere and the ocean. Most of these parameterizations are based on results from the atmospheric boundary layer over land and do not account for complications associated with the free surface of the ocean. Consequently, air–sea exchanges may be severely underestimated. For example, the momentum flux (wind stress) into the ocean is commonly parameterized by using the so-called wind mixing coefficient. The wide range of variation in the values of this coefficient (e.g., Table 1 in Huang 1986) is in part a reflection of wave effects (e.g., breaking). As pointed out by Huang, the fundamental problem is that using the friction velocity in water, $u_* = \sqrt{\tau_0/\rho_w}$ (τ_0 is the surface wind stress and ρ_w is the density of sea water), alone for parameterization amounts to neglecting the dynamical characteristics of the surface layer that are influenced by the wave conditions, especially breaking waves. A different example of the importance of wave breaking is the role played in gas transfer across the air–water interface (e.g., Thorpe 1982). In an important paper by Kitaigorodskii (1984), it was shown that in order to correctly describe gas transfer in the liquid near the air–sea interface, the structure of the

Corresponding author address: Dr. Jim N. Moum, College of Oceanic and Atmospheric Sciences, Oregon State University, Oceanography Administration Bldg. 104, Corvallis, OR 97331-5503.
E-mail: moum@oce.orst.edu

turbulence in turbulent patches created by breaking waves needs to be considered. His proposed theory indicates that the appropriate gas transfer velocity, V_{tr}, is dependent on the turbulence kinetic energy (TKE) dissipation rate, ϵ, in the turbulent patch such that $V_{tr} \propto \epsilon^{1/4}$.

To date, studies carried out in the ocean, lakes, and laboratories show that in many cases the aquatic boundary layer has similar scaling laws (for definition of scaling laws see section 4a) to those in the atmospheric boundary layer (ABL) over land [the ABL is commonly defined as that part of the atmosphere bounded by the land surface below and by the first temperature inversion above (e.g., Stull 1988)]. Some investigators have shown that wind-driven near-surface layers of oceans and lakes exhibit scaling laws consistent with constant stress layers over solid boundaries. Jones and Kenney (1977) found that turbulence velocity fluctuations appear to have a velocity scale proportional to the friction velocity in water and a length scale proportional to the depth, z. Surface velocity measurements using drifters and drogues (Churchill and Csanady 1983) showed the velocity to decrease nearly logarithmically with depth from the surface to a depth of about 1 m. Field measurements in a freshwater lake (e.g., Dillon et al. 1981) and in the ocean (Soloviev et al. 1988, 1989) showed that $\epsilon(z)$ scales as $u_*^3/\kappa z$ (von Kármán's constant, $\kappa \approx 0.4$). Lombardo and Gregg (1989) observed a range of conditions in a convective OBL, concluding that ϵ could be normalized very well by the sum of convective and surface-layer (SL) similarity scalings. Scaling of χ was less successful and applied only in part of the OBL when turbulent production was dominated either by convection or wind stress.

On the other hand, evidence for enhanced turbulence and mixing in the upper part of the aquatic BL comes from a growing number of experimental field and laboratory studies. Field studies in the upper part of the OBL under different forcing conditions (Stewart and Grant 1962; Shay and Gregg 1984; Gregg 1987; Gargett 1989; Anis and Moum 1992; Osborn et al. 1992) showed enhanced TKE dissipation rates much larger than predicted by SL and/or convective scalings. Kitaigorodskii et al. (1983) and Agrawal et al. (1992) reported enhanced dissipation rates beneath surface waves, observed during two separate field experiments in Lake Ontario. Thorpe (1984), using acoustic measurements of bubbles near the surface of the ocean, suggested the importance of turbulence generated by breaking waves. In a laboratory experiment with no imposed winds, Rapp and Melville (1990) showed that, as a result of wave breaking, mean surface currents in the range 0.02–$0.03C$ (where C is the characteristic phase speed) were generated and took about 60 wave periods to decay to $0.005C$. Turbulence rms velocities on the order of $0.02C$ were measured, decaying to $0.005C$ after more than 60 wave periods, and were still significant to a depth of k^{-1} (where k is the characteristic wavenumber). In light of these experiments it seems plausible that breaking surface waves are an important source of TKE and mixing in the OBL, and, therefore, should be considered more thoroughly.

Another source of TKE may be associated with downward wave momentum flux. Shonting (1964, 1967, 1968, 1970), Cavaleri et al. (1978), Cavaleri and Zecchetto (1985), and Yefimov and Khristoforov (1969, 1971) observed in field experiments that horizontal and vertical wave velocities were consistently out of quadrature, resulting in a net downward wave momentum flux. Similar results, from laboratory experiments, were reported by Dobroklonskiy and Lesnikov (1975) and by Bliven et al. (1984), who also showed that TKE decayed exponentially with depth, penetrating to a depth on the order of the wavelength. In a recent laboratory experiment, Cheung and Street (1988) carefully examined turbulence in the water at an air–water interface for different cases of surface gravity waves. They showed that, although turbulence parameters followed constant stress-layer scaling in the case of wind-generated waves, they behaved very differently in the case of wind-ruffled mechanically generated waves, for which 1) increased turbulence levels were observed, away from the surface to a depth of about $1/k$ (k is the wavenumber of the mechanically generated waves), and the depth decay of turbulence rms velocities followed the decay of wave rms velocities closely; 2) the phase difference between $\tilde{u}$ and $\tilde{w}$, the horizontal and vertical wave velocities, respectively, was consistently less than 90°; 3) in both the wind-ruffled mechanically generated waves and the high wind speed wind wave experiments, the mean velocity profiles (as a function of depth) had slopes smaller than predicted for turbulent boundary layers near a solid surface, suggesting that the waves affect the mean flow. An ocean with swell and wind waves might closely resemble the laboratory wind-ruffled mechanically generated waves of Cheung and Street's experiment. If this is true, we might expect that for a combination of swell and wind waves the layer near the surface of the ocean will reveal similar departures of turbulence from the predicted behavior of a turbulent boundary layer near a solid surface.

Although the recent experimental field and laboratory studies, referred to above, provide the most convincing evidence of the importance of surface waves in the dynamics of the upper OBL, treatment of wave–turbulence interactions started much earlier. More than 40 years ago Bowden (1950) suggested, on dimensional grounds, an eddy viscosity as a function of wave parameters to explain the observed rate of decay of ocean swell. Phillips (1961) suggested the generation of a turbulent vortex field by the straining of fluid elements associated with nonbreaking random wave motion;

however, the intensity of turbulence was of second order and too weak to account for wave attenuation or mixing in the OBL. Kitaigorodskii (1961), using dimensional arguments, proposed an eddy viscosity coefficient based on the vertical shear of the wave orbital velocity to calculate the vertical temperature profile in the upper OBL. Jacobs (1978), using numerical simulations with alternative forms of eddy viscosity coefficients, showed that an eddy viscosity based on Kitaigorodskii's (1961) formulation proved to be significantly better in predicting the vertical temperature structure when compared to observations carried out during the Barabados Oceanographic and Meteorological Experiment (BOMEX). Benilov (1973), again using dimensional reasoning, proposed analytic expressions for TKE and ϵ as functions of depth and sea state, assuming surface waves as the main source of turbulence. Benilov's model was used by Soloviev (1986) to explain observations of ϵ made in the upper Atlantic OBL. Huang (1986) proposed an exponential depth decay of $\epsilon(z)$ by assuming a similar depth decay of TKE and wave KE; however, a solid physical explanation for this assumption was not presented.

In the following we examine results from turbulence profiling measurements in the OBL, conducted under different meteorological and sea conditions. In section 2 the necessary theoretical background and the governing equations are presented. Experimental details, meteorological conditions, observational results, and some statistical aspects of the data are presented in section 3. In section 4 we discuss the TKE equation in the absence of surface waves. In section 5 we discuss the effects of surface waves on TKE and, consequently, $\epsilon(z)$; possible scalings for $\epsilon(z)$ are derived. A synopsis of recent near-surface turbulence measurements is presented in section 6. Conclusions and a summary are presented in section 7.

2. Theoretical background

a. General considerations

Unlike the rigid boundary of the ABL over land, the OBL is bounded by a free surface through which momentum, heat, and gas are exchanged with the lower atmosphere. In the traditional treatment of boundary layers, the equations of momentum and continuity are treated without inclusion of surface waves. However, the existence of the free surface, with waves as an intermediary in the momentum and energy exchange with the atmosphere, has to be taken into account when considering the OBL.

To explicitly separate the relative influences of mean, wave, and turbulence components of the flow field, we decompose all variables (e.g., velocity, pressure) of the flow as

$$a = \bar{a} + \tilde{a} + a', \tag{1}$$

where $\bar{a}$ is the time-average component, $\tilde{a}$ the periodic wave-induced component, and a' the turbulence component of the motion. Time averages are understood to be performed over timescales much larger than the characteristic wave period. From the definition of the time average and assuming that the mean, the periodic wave-induced, and the turbulence components of the motion are uncorrelated, we have

$$\bar{\tilde{a}} = 0, \quad \overline{a'} = 0, \quad \overline{\tilde{a}\tilde{b}} = 0, \quad \overline{\tilde{a}b'} = 0, \quad \overline{\tilde{a}b'} = 0, \tag{2}$$

where b represents some other flow variable, including a.

In the following analysis an incompressible Boussinesq flow is assumed, and the summation notation in a right-hand Cartesian system is used. Then, using (1) and (2), the continuity equation for the mean component of the flow, $\bar{U}_i$, is

$$\frac{\partial \bar{U}_i}{\partial x_i} = 0, \tag{3}$$

and the momentum equation for the mean flow is

$$\frac{\partial \bar{U}_i}{\partial t} + \bar{U}_j \frac{\partial \bar{U}_i}{\partial x_j} = -\frac{1}{\rho}\frac{\partial \bar{P}}{\partial x_i} - \delta_{i3} g + \nu \frac{\partial^2 \bar{U}_i}{\partial x_j^2} - \frac{\partial}{\partial x_j}(\overline{u_j' u_i'}) - \frac{\partial}{\partial x_j}(\overline{\tilde{u}_j \tilde{u}_i}). \tag{4}$$

The last term on the right-hand side of this equation represents the interaction of the wave field with the mean flow. Similarly, the continuity equation for the combined wave–turbulence component of the flow, $u_i^{w,t} = \tilde{u}_i + u_i'$, is

$$\frac{\partial u_i^{w,t}}{\partial x_i} = 0, \tag{5}$$

and the momentum equation is

$$\frac{\partial u_i^{w,t}}{\partial t} + \bar{U}_j \frac{\partial u_i^{w,t}}{\partial x_j} = -\frac{1}{\rho}\frac{\partial p^{w,t}}{\partial x_i} - \delta_{i3} g \frac{\rho'}{\rho} - \frac{\partial}{\partial x_j}(u_j^{w,t} \bar{U}_i) - \frac{\partial}{\partial x_j}(u_j^{w,t} u_i^{w,t}) + \nu \frac{\partial^2 u_i^{w,t}}{\partial x_j^2} + \frac{\partial}{\partial x_j}(\overline{u_j' u_i'}) + \frac{\partial}{\partial x_j}(\overline{\tilde{u}_j \tilde{u}_i}). \tag{6}$$

To assess the possible interactions between mean, wave, and turbulence components of the flow it is necessary to examine the respective KE equations. We consider this problem in the following two sections. In section 2b we consider an irrotational wave field, derived from a scalar velocity potential. We use an irrotational wave field firstly to demonstrate that one of the two wave–turbulence interaction mechanisms we propose (section 5b) may exist in an irrotational wave field, and secondly, irrotationality is used as a means

of separating the three components of the flow. In section 2c we assume a rotational wave field, observed in field (e.g., Cavaleri et al. 1978) and laboratory (e.g., Cheung and Street 1988) experiments, to develop the necessary background for the second wave–turbulence interaction mechanism proposed. In the case of a rotational wave field, the phase-averaging technique is used to separate the mean, wave-induced, and turbulence components of the flow.

b. Turbulence in an irrotational wave field

We assume an irrotational wave field, $\tilde{u}_i = \partial\Phi/\partial x_i$, and a rotational turbulence field, $u_i' = \epsilon_{ijk}\partial V_k/\partial x_j$, where Φ and $\mathbf{V}$ are, respectively, the scalar and vector velocity potentials (e.g., Kitaigorodskii and Lumley 1983). For simplicity, we consider a statistically homogeneous flow in the horizontal plane with the x axis aligned in the direction of the mean flow, so that $\bar{U}_i = [U(z, t), 0, 0]$, $\bar{P} = P(z, t)$, and a wave field propagating in the x direction.

The mean kinetic energy (MKE) equation, obtained by multiplying (4) by $\bar{U}_i$, averaging and using the assumptions above, is

MKE:

$$\frac{\partial}{\partial t}\left(\frac{1}{2}\overline{UU}\right) = +\nu\bar{U}\frac{\partial^2\bar{U}}{\partial z^2} - \frac{\partial}{\partial z}(\overline{w'u'\bar{U}}) + \overline{w'u'}\frac{\partial\bar{U}}{\partial z}. \tag{7}$$

The wave kinetic energy (WKE) equation, obtained by multiplying Eq. (6) by $\tilde{u}_i$, averaging, and using (2), is

WKE:

$$\frac{\partial}{\partial t}\left(\frac{1}{2}\overline{\tilde{u}_i\tilde{u}_i}\right) = -\overline{\tilde{u}_i\tilde{u}_j}\frac{\partial\bar{u}_i'}{\partial x_j} - \frac{\partial}{\partial z}\left(\overline{w'\frac{1}{2}\tilde{u}_i\tilde{u}_i}\right) - \frac{\partial}{\partial z}(\overline{w'u_i'\tilde{u}_i}) + \overline{u_i'u_j'}\frac{\partial\tilde{u}_i}{\partial x_j}. \tag{8}$$

Note that the molecular wave diffusion term, $\nu\partial^2\tilde{u}_i/\partial x_j^2$, vanishes because the wave field satisfies Laplace's equation and the transport term, $\overline{\tilde{u}_j\partial(\tilde{p}/\rho + {}^1/_2\tilde{u}_i\tilde{u}_i)/\partial x_j}$, vanishes by the assumption of an irrotational wave field. The TKE equation, obtained by multiplying Eq. (6) by u_i' and averaging, is

TKE:

$$\frac{\partial}{\partial t}\left(\frac{1}{2}\overline{u_i'u_i'}\right) = -\frac{\partial}{\partial z}\left[\overline{w'\left(\frac{p'}{\rho} + \frac{1}{2}u_i'u_i'\right)}\right] - \frac{g}{\rho}\overline{w'\rho'} - \overline{w'u'}\frac{\partial\bar{U}}{\partial z} - \frac{\partial}{\partial z}\left(\overline{w'\frac{1}{2}\tilde{u}_i\tilde{u}_i}\right) - \frac{\partial}{\partial z}\left(\overline{\tilde{w}\frac{1}{2}u_i'u_i'}\right) - \overline{u_i'u_j'}\frac{\partial\tilde{u}_i}{\partial x_j} - \epsilon, \tag{9}$$

where we have used (2), our above assumptions, and the definition $\epsilon = \nu\overline{(\partial u_i'/\partial x_j)^2}$ for the TKE dissipation rate. We have dropped the term $\nu\partial^2(\frac{1}{2}\overline{u_i'u_i'})/\partial x_j^2$ from the TKE equation since we expect it to be several orders of magnitude smaller than the other terms in the TKE budget (e.g., Tennekes and Lumley 1972).

c. Turbulence in a rotational wave field

Although in many cases the surface wave field is assumed to be irrotational, a number of field and laboratory studies have shown instances where the surface wave field departed from irrotationality. The earliest reports are from Shonting's observations of the velocities beneath the ocean free surface (1964, 1967, 1968, 1970). These observations showed the vertical and horizontal wave orbital velocities to be out of quadrature, leading to a downward momentum flux that decayed rapidly with depth. Similar results from field observations were reported by Cavaleri et al. (1978) and Cavaleri and Zecchetto (1985). Yefimov and Khristoforov (1969, 1971) found that the most important contribution to the large vertical momentum fluxes they observed in the near-surface layer was due to the swell, since the frequency spectrum of the wave stress coincided with the frequency spectrum of the swell. Laboratory studies by Dobroklonskiy and Lesnikov (1975) showed similar results of large wave stresses due to the nonorthogonality of the horizontal and vertical wave velocities. In their laboratory studies Cheung and Street (1988) found that the wave-induced stress $-\tilde{w}\tilde{u}$ in wind wave experiments was generally negative but smaller in magnitude than the turbulence Reynolds stress, $-\overline{w'u'}$. However, in the case of wind-ruffled mechanically generated waves, the wave-induced stress was negative and larger in magnitude than the turbulence Reynolds stress, resulting in energy transfer from the wave field to the mean flow through the term $\tilde{w}\tilde{u}\partial\bar{U}/\partial z$ [see Eq. (15)]. Another laboratory study (Bliven et al. 1984) showed that the Reynolds stress increased with wave steepness and decreased exponentially with depth.

Due to the apparent departure of the wave field from the classical notion of irrotationality, we cannot use the same wave–turbulence separation method as in section 2b. However, separation can be achieved by the phase-averaging technique (Hussain and Reynolds 1970). This method is suitable for extracting the wave-induced motion when the wave field is characterized by a specific wavelength in the spectrum. An example is the laboratory case of wind-ruffled mechanically generated waves (Cheung and Street 1988), or the ocean in which the surface wave field is a combination of wind waves and dominant swell. It should be noted that the turbulence component of the flow in this case may include random wave components that are mainly attributed to short wind waves and, therefore, impor-

tant only close to the surface of the ocean. If on the other hand the wave field is completely random—for example, wind waves in a fetch-limited lake when swell is absent—the phase-averaging technique fails.

The phase average, $\langle a \rangle$, is defined as the average over a large ensemble of values of a that are realized at some specified phase of the reference wave. From this definition and the definition of the time average, we have the following properties used in deriving the equations to follow:

$$\langle a \rangle = \tilde{a} + \bar{a}, \quad a' = a - \langle a \rangle,$$
$$\langle a' \rangle = 0, \quad \langle \bar{a} \rangle = \overline{\langle a \rangle} = \bar{a},$$
$$\langle \tilde{a}b \rangle = \tilde{a}\langle b \rangle, \quad \text{and} \quad \langle \bar{a}b \rangle = \bar{a}\langle b \rangle. \tag{10}$$

Phase averaging the continuity equation for the combined fluctuating component (5) results in separate continuity equations for wave and turbulence components of the motion;

$$\frac{\partial \tilde{u}_i}{\partial x_i} = 0, \tag{11}$$

and

$$\frac{\partial u_i'}{\partial x_i} = 0, \tag{12}$$

where (12) is produced by subtracting (11) from (5). Phase averaging the momentum equation for the combined fluctuating component of the motion (6), and using (11) and (12), we obtain the wave momentum equation

$$\frac{\partial \tilde{u}_i}{\partial t} + \bar{U}_j \frac{\partial \tilde{u}_i}{\partial x_j} + \tilde{u}_j \frac{\partial \bar{U}_i}{\partial x_j} = -\frac{1}{\rho}\frac{\partial \tilde{p}}{\partial x_i} + \nu \frac{\partial^2 \tilde{u}_i}{\partial x_j^2} + \frac{\partial}{\partial x_j}(\overline{u_j' u_i'} - \langle u_j' u_i' \rangle) + \frac{\partial}{\partial x_j}(\overline{\tilde{u}_j \tilde{u}_i} - \tilde{u}_j \tilde{u}_i). \tag{13}$$

Subtraction of the wave momentum equation (13) from the momentum equation for the combined fluctuating component (6), and using (12), results in the momentum equation for turbulence in the presence of waves

$$\frac{\partial u_i'}{\partial t} + \bar{U}_j \frac{\partial u_i'}{\partial x_j} + \tilde{u}_j \frac{\partial u_i'}{\partial x_j} + u_j' \frac{\partial \bar{U}_i}{\partial x_j} + u_j' \frac{\partial \tilde{u}_i}{\partial x_j} = -\frac{1}{\rho}\frac{\partial p'}{\partial x_i} - \delta_{i3} g \frac{\rho'}{\rho} + \nu \frac{\partial^2 u_i'}{\partial x_j^2} + \frac{\partial}{\partial x_j}(\langle u_j' u_i' \rangle - u_j' u_i'). \tag{14}$$

The KE equations for the mean, wave, and turbulence components of the flow are obtained by multiplying the momentum equations (4), (13), and (14) by $\bar{U}_i$, $\tilde{u}_i$, and u_i', respectively, and then phase and time averaging. Assuming, as before, statistical homogeneity in the horizontal plane, and taking the x axis in the direction of the mean current, results in the following equations for MKE, WKE, and TKE.

MKE:

$$\frac{\partial}{\partial t}\left(\frac{1}{2}\overline{\bar{U}\bar{U}}\right) = +\nu \bar{U}\frac{\partial^2 \bar{U}}{\partial z^2} - \frac{\partial}{\partial z}(\overline{w'u'\bar{U}}) + \overline{w'u'}\frac{\partial \bar{U}}{\partial z} - \frac{\partial}{\partial z}(\overline{\tilde{w}\tilde{u}\bar{U}}) + \overline{\tilde{w}\tilde{u}}\frac{\partial \bar{U}}{\partial z}, \tag{15}$$

WKE:

$$\frac{\partial}{\partial t}\left(\frac{1}{2}\overline{\tilde{u}_i\tilde{u}_i}\right) = -\frac{\partial}{\partial z}\left[\overline{\tilde{w}\left(\frac{\tilde{p}}{\rho} + \frac{1}{2}\tilde{u}_i\tilde{u}_i\right)}\right] + \nu\overline{\tilde{u}_i\frac{\partial^2 \tilde{u}_i}{\partial x_j^2}} - \overline{\tilde{w}\tilde{u}}\frac{\partial \bar{U}}{\partial z} - \frac{\partial}{\partial z}(\overline{\langle w'u_i' \rangle \tilde{u}_i}) + \overline{\langle u_i'u_j' \rangle \frac{\partial \tilde{u}_i}{\partial x_j}}, \tag{16}$$

TKE:

$$\frac{\partial}{\partial t}\left(\frac{1}{2}\overline{u_i'u_i'}\right) = -\frac{\partial}{\partial z}\left[\overline{w'\left(\frac{p'}{\rho} + \frac{1}{2}u_i'u_i'\right)}\right] - \frac{g}{\rho}\overline{w'\rho'} - \overline{w'u'}\frac{\partial \bar{U}}{\partial z} - \frac{\partial}{\partial z}\left[\overline{\tilde{w}\left\langle\frac{1}{2}u_i'u_i'\right\rangle}\right] - \overline{\langle u_i'u_j' \rangle \frac{\partial \tilde{u}_i}{\partial x_j}} - \epsilon. \tag{17}$$

The term $\nu\partial^2(\frac{1}{2}\overline{u_i'u_i'})/\partial x_j^2$ was neglected from the TKE equation as before.

Experimental field results are presented in the next section to illustrate the behavior of turbulence observed in the OBL under different surface-forcing conditions. The observational results will be discussed in sections 4 and 5 in the context of the theoretical background presented above.

3. Observations

a. Experimental details

This study is based on two experiments conducted under different atmospheric forcing and sea state conditions. Vertical profiles were made using the microstructure profiler Chameleon (Moum et al. 1995). This instrument provides microscale measurements of temperature and conductivity, from which salinity and density were computed, and microscale velocity shear, from which $\epsilon(z)$ was computed. The physical size of the airfoil probes (diameter 0.4 cm; length 1.4 cm) poses an upper limit on the spatial resolution of the microscale velocity structure, and the inherent spatial averaging of the probe results in an underestimate of

TABLE 1. Daytime and nighttime averaged values of the atmospheric and sea state conditions for the OR89 and OR90 experiments. Surface wind stress, τ_0; surface heat flux, J_q^0 (positive upward); and surface buoyancy flux, J_b^0 (positive upward), were determined from bulk aerodynamic formulas (Large and Pond 1981). The Monin–Obukhov length scale is defined as $L \equiv -u_*^3/\kappa J_b^0$, where $u_* \equiv \sqrt{\tau_0/\rho_w}$ is the friction velocity in water, ρ_w is the density of seawater, and $\kappa = 0.4$ is von Kármán's constant; L is negative during convection. The significant wave height, H_s, and period, T, are from R/V *Wecoma*'s ship's officers' log and are given for swell and wind waves.

	Number of profiles	τ (N m^{-2})	J_q^0 (W m^{-2})	$10^7 J_b^0$ (m^2 s^{-3})	L (m)	Swell H_s (m), T (s)	Wind waves H_s (m), T (s)
OR89							
night 1	29	0.25	223	1.4	−67.7	3.0, 12 2.5, 6	1.0, 4 —
night 2	20	0.11	73	0.4	−63.0	2.0, 6–8	0.6, 4–5
OR90							
day 1	10	0.05	−32	−0.2	49.5	1.2–1.5, —	wavelets
day 2	9	0.14	−266	−1.7	31.1	1.8, 6	0.9, 4
night 1	9	0.23	197	1.4	−57.8	1.8–2.1, 5	0.9, 4
night 2	43	0.12	124	0.6	−49.8	2.1–1.8, 6	0.9–0.6, 4–3
night 3	40	0.03	42	0.2	−26.0	1.8, 7–8	0.3, 1–2

the true dissipation. Because the shear spectrum shifts to smaller scales as ϵ increases, the error due to the spatial averaging of the probe increases with the dissipation level. The probe's response was corrected by applying an empirical transfer function (Ninnis 1984) to the measured estimates of the TKE dissipation rates. Estimates of ϵ were also corrected for variance lost due to incomplete resolution of the shear spectrum by comparing to the universal form of Nasmyth (1970). [The full procedure is described by Moum et al. (1995).]

The two experiments were conducted off the Oregon coast during the summers of 1989 and 1990, hereafter OR89 and OR90, in water depths between 1000 and 2000 m. Chameleon, deployed from R/V *Wecoma*, was lowered with the aid of an attached weight, which upon release caused the instrument to freely rise, due to its positive buoyancy, while taking microstructure measurements on its way to the ocean surface. During profiling, the ship was steered so as to keep the bow into the wind. Speeds were kept at a minimum, so virtually no progress was made over ground, as the windage on the ship nearly balanced ship propulsion. The profiler was lowered to about 120-m depth (usually deeper, sometimes shallower) and allowed to stay there for a minute or two before weights were released and it began its ascent. During this time, whatever subsurface currents were present in the water column invariably caused a sideward drift of the profiler, taking it away from the ship. The profiler was spotted visually to surface at about 150–200-m distance and virtually always well to one side of the ship. In cases when the profiler was suspected to have surfaced anywhere near the wake (approximately 15% of the profiles), the profiles were not used in our analysis. The profiles used are believed, therefore, to be free from contamination by the ship's wake up to the surface. For analysis, we used data starting at a depth of 0.5 m.

Continuous shipboard measurements of meteorological parameters were taken and included wind velocity, air temperature, and humidity, solar and longwave radiation, and sea surface temperature and conductivity. Surface wind stress τ_0, surface heat flux J_q^0, and surface buoyancy flux J_b^0 were calculated using bulk aerodynamic formulas (Large and Pond 1981). The significant wave height, H_s, and periods of swell and wind waves and their direction were estimated by the mate on watch every 15 min during OR89 and every hour during OR90. Single estimates of the significant wave height are to the nearest foot, and an uncertainty of ±0.3 m may be expected. However, for each day or night we averaged at least 5–6 wave height estimates, reducing the uncertainty in the average wave height to about 0.1 m.

The depth of the OBL, for daytime and nighttime, was estimated subjectively from individual profiles of salinity, θ, and σ_θ, and then averaged for the respective day or night. This resulted in OBL depths, D, roughly equivalent to the depth at which σ_θ exceeded the surface value by 0.005 kg m^{-3}. For OR89, when salinity estimates were unavailable, the OBL depth is the depth at which θ was exceeded by the surface value by 0.01 K.

b. Oregon 1989

Data for this experiment consists of 29 successful profiles collected during the first night and of 20 profiles from the second night, a couple of days later. Since no conductivity sensor was mounted on Chameleon, the stability of the OBL was inferred from the structure of the vertical potential temperature profile.

During the first night the average surface buoyancy flux was 1.4×10^{-7} m^2 s^{-3} and strong steady northerly winds ($\sim$13 m s^{-1}) produced an average surface stress of 0.25 N m^{-2} (Table 1). Sea state was dominated by

two swells: one, heavy, from NW with a period of about 12 s and 3.0-m significant wave height and the other from NNW with a shorter period of 6 s and significant height of 2.5 m. Intense breaking, mainly of wind waves with significant height of about 1 m, took place throughout the night. The profile of θ for this night (Fig. 1a) shows a neutrally stratified layer in the upper 10 m or so of the OBL with a sharp thermocline beneath it. TKE dissipation rates, between the surface and the thermocline, were higher than could be accounted for by the wind stress production term, $u_*^3/\kappa z$.

Meteorological and sea state conditions during the second night were substantially different and relatively moderate compared to the rough conditions of the first night. The average surface buoyancy flux was 0.4

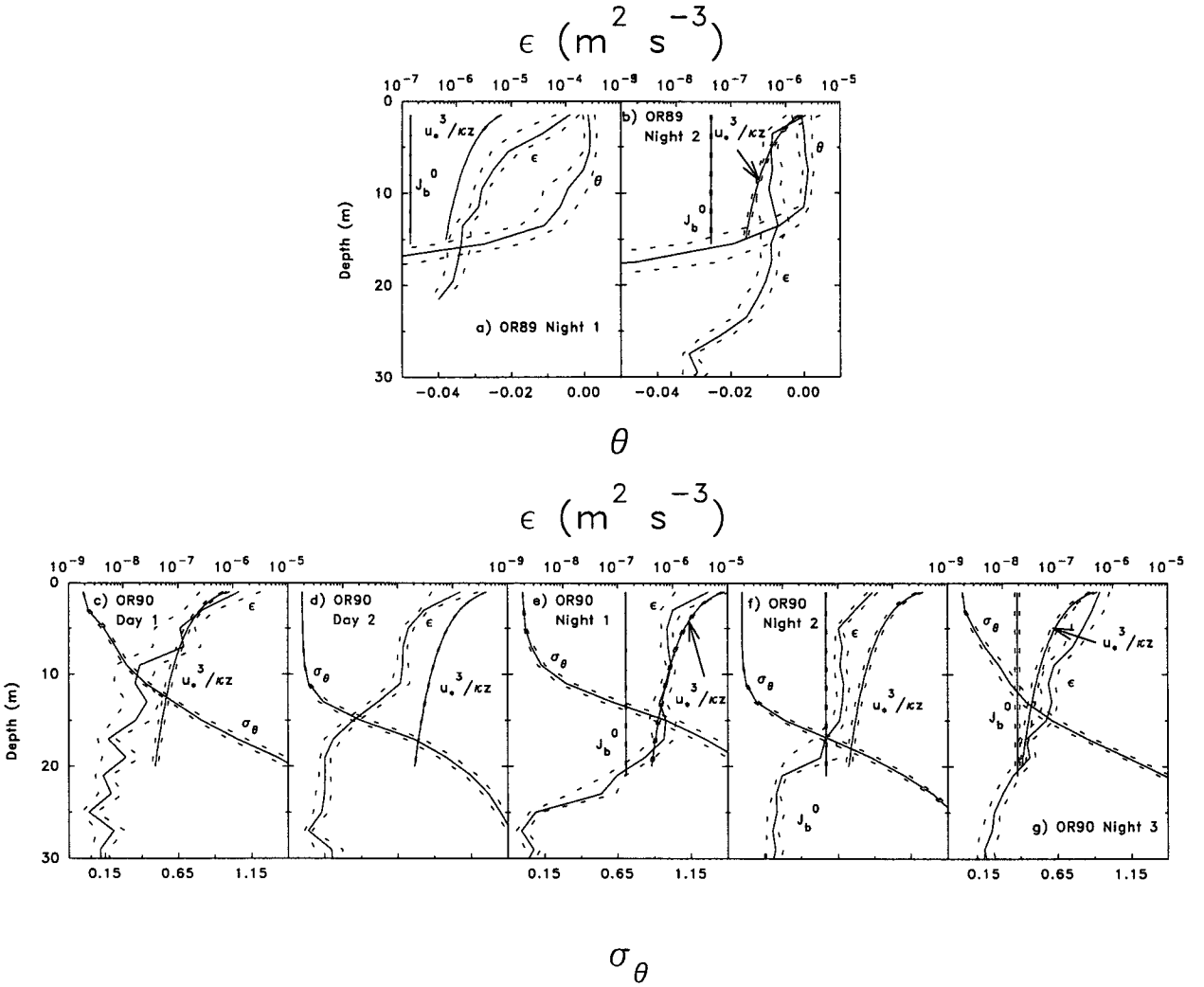

FIG. 1. Referenced and averaged profiles of potential density, σ_θ, and TKE dissipation rate, ϵ. Here σ_θ is defined as $\rho_w(s, \theta, 0) - 1000$ kg m^{-3}, where ρ_w, the density of seawater at atmospheric pressure (i.e., $p = 0$), is given as a function of salinity, s, and potential temperature, θ. The effect of adiabatic heating or cooling is removed by using θ instead of the in situ temperature and is useful when comparing fluid parcels at different depths. The number of profiles in each average and atmospheric and sea state conditions are presented in Tables 1 and 2. For comparison purposes, the influence of horizontal gradients was removed as follows: values of σ_θ (or θ for OR89) for single profiles were first referenced to their average value in the OBL and then depth binned and averaged. Depth bins are 2 m for all datasets. Also plotted are $u_*^3/\kappa z$ and the nighttime surface buoyancy flux, J_b^0. Dotted lines represent the 95% bootstrap confidence limits (Efron and Gong 1983). Panels (a, b) are for OR89 profiles. No conductivity sensor was mounted on the profiler during this experiment; hence the referenced potential temperature (θ) profile is presented instead of σ_θ (a constant salinity value from conductivity measurements at 5-m depth was used in the calculation of θ). During night 1 (a), when winds and seas were high (Table 1), the dissipation rate in the neutral OBL was larger than the wind stress production, $u_*^3/\kappa z$, while during night 2 (b), when conditions were moderate, $\epsilon(z)$ scaled with $u_*^3/\kappa z$ in the upper 10 m of the OBL. The somewhat higher values of ϵ near the base of the OBL during the second night may be due to processes not related directly to wind forcing such as entrainment (note the different range of values of the ϵ axes for the two nights). Panels (c)–(g) are for OR90 profiles.

$\times 10^{-7}$ m^2 s^{-3} and winds, decreasing from 10.0 to 8.0 m s^{-1}, produced an average surface stress of 0.11 N m^{-2}. A 2.0-m swell with a period of 6–8 s and wind waves of 0.6 m (Table 1), breaking only sporadically, defined the sea state. A neutrally stratified layer, extending from the surface to an average depth of about 12 m, was capped below by a sharp thermocline (Fig. 1b). In the upper 10 m of the OBL, ϵ followed the predicted constant stress-layer scaling within 95% confidence limits but had slightly larger values deeper, possibly due to entrainment at the base of the OBL.

c. *Oregon 1990*

The results reported in this section are from a set of 111 profiles, collected during two daytime and three nighttime profiling sessions. During the experiment, meteorological conditions varied from periods with very light winds and no wind waves to periods with strong winds and breaking waves.

The first set of 10 profiles was taken in late afternoon, when winds were 5–6 m s^{-1}, after rising steadily from 1 m s^{-1} during a period of about 5 h. Swell was 1.2–1.5 m in height, while wind waves were mainly nonbreaking wavelets (Table 1). A stable OBL, 2.1 m deep and with an average density gradient $\overline{\sigma_{\theta_z}}$ of -23.89×10^{-4} kg m^{-4} (Table 2), was established during the day when the surface of the ocean was being heated and winds were light. Although stably stratified, $\epsilon(z)$ followed $u_*^3/\kappa z$ up to a depth of about 8 m, below which $\epsilon(z)$ decreased by almost an order of magnitude (Fig. 1c).

Another set of daytime casts was carried out in late afternoon 5 days later. Steady winds of 10 m s^{-1}, after rising slowly from 8 m s^{-1} during a 5-h period, produced an average stress of 0.14 N m^{-2} (Table 1). A swell with 1.8 m significant height and a period of 6 s, and wind waves with 0.9 m significant height and periods between 3 and 4 s and occasional whitecaps, defined the sea state. The OBL was deeper (7.7 m) and slightly less stratified than the first day, and the average value of σ_{θ_z} was -10.08×10^{-4} kg m^{-4}. Here $\epsilon(z)$ was smaller than $u_*^3/\kappa z$ and decreased by almost two orders of magnitude near the base of the OBL (Fig. 1d).

The first nighttime set consisted of nine profiles taken during the early night hours (19–21 local). Winds, 11.5–12.5 m s^{-1}, were in the last phase of a rising trend from 2 to 13.5 m s^{-1} and the average surface buoyancy flux was 1.4×10^{-7} m^2 s^{-3}. Sea state was developing from a 1.2- to a 1.8–2.1 m swell with a 5-s period, and wind waves rose from ripples to waves of 0.9-m height and 4-s period with some whitecaps (Table 1). The average value of σ_{θ_z} in the OBL ($D = 4.1$ m) was -16.08×10^{-4} kg m^{-4}, and $\epsilon(z)$ was slightly smaller than $u_*^3/\kappa z$ (Fig. 1e). Between 8 and 18 m, $\epsilon(z) \sim u_*^3/\kappa z$, while deeper than 18 m, ϵ decreased rapidly by more than two orders of magnitude.

During the first part of the second night, winds averaged 10.5 m s^{-1} and then dropped in a couple of hours to an average of 7.5 m s^{-1}. Swell decreased in height from 2.1 to 1.8 m and wind waves decreased in period from 4 to 3 s and from 1.2 to 0.6–0.3 m (Table 1). The 10.1-m deep OBL was only slightly stable with an average value of σ_{θ_z} of -2.99×10^{-4} kg m^{-4} (Table 2). TKE dissipation rate was smaller than $u_*^3/\kappa z$ throughout the OBL (Fig. 1f).

Relatively weak winds of about 5 m s^{-1} prevailed during most of the third night, an exception being one

TABLE 2. Daytime and nighttime values of OBL parameters for OR89 and OR90. Here D is the OBL thickness; D/L is a bulk stability parameter; $u_* \equiv \sqrt{\tau_0/\rho_w}$ is the ocean surface friction velocity; $\theta_* \equiv -J_q^0/\rho_w C_p u_*$ is the ocean surface temperature scale (C_p is the specific heat); $\overline{\theta_z}$ and $\overline{\sigma_{\theta z}}$ are the mean vertical gradients of the potential temperature θ and the potential density σ_θ, respectively, and were evaluated by a linear regression to the curves of θ and σ_θ of each profile and then averaged for the day or the night (θ and σ_θ are defined in the caption of Fig. 1); $-z/L$ is a surface-layer stability parameter (positive, when $L > 0$, implies statically stable and negative, when $0 > L$, implies statically unstable); $\Phi_h \equiv (\kappa z/\theta_*)\overline{\theta_z}$ is a dimensionless temperature gradient; $\int \rho\epsilon dz / \int (\rho u_*^3/\kappa z) dz$ is the ratio of the depth-integrated dissipation rate to the depth integrated wind stress production. The quantities $\overline{\theta_z}$, $\overline{\sigma_{\theta z}}$, $\int \rho\epsilon dz / \int (\rho u_*^3/\kappa z) dz$, $-z/L$, and Φ_h were estimated for the depth interval -0.5 m $> z > -D$.

	D (m)	D/L	$10^2 u_*$ (m s^{-1})	$10^2\theta_*$ (K)	$10^4\overline{\theta_z}$ (K m^{-1})	$10^4\overline{\sigma_{\theta z}}$ (kg m^{-4})	$-z/L$	Φ_h	$\frac{\int \rho\epsilon dz}{\int (\rho u_*^3/\kappa z) dz}$
OR89									
night 1	13.5	−0.24	1.57	−0.35	8.07	—	(−0.24)–(−0.01)	0.05–1.26	13.0
night 2	14.5	−0.31	1.04	−0.17	3.23	—	(−0.31)–(−0.01)	0.04–1.08	1.3
OR90									
day 1	2.1	0.06	0.67	0.12	38.81	−23.89	0.01–0.06	0.67–2.80	1.9
day 2	7.7	0.25	1.18	0.55	28.68	−10.08	0.02–0.25	0.10–1.60	0.3
night 1	4.1	−0.07	1.49	−0.32	35.21	−16.08	(−0.07)–(−0.01)	0.22–1.78	0.5
night 2	10.1	−0.27	1.08	−0.28	12.08	−2.99	(−0.27)–(−0.01)	0.09–1.73	0.2
night 3	3.7	−0.24	0.56	−0.18	15.02	−3.89	(−0.24)–(−0.02)	0.16–1.22	1.8

hour at the beginning when winds rose from 2.5 m s^{-1} to 5 m s^{-1} and one hour at the end when winds decreased to 3.5 m s^{-1}. The surface buoyancy flux was the smallest of all nights, averaging 0.2×10^{-7} m^2 s^{-3} (Table 1). A swell with 1.8-m significant height and a period of 6–7 s and wind waves less than 0.3 m in height with periods between 1 and 2 s defined the sea state. No whitecaps were noticed. The OBL (D = 3.7 m) was slightly stably stratified with $\overline{\sigma_{\theta_z}} = -3.89 \times 10^{-4}$ kg m^{-4}. Here $\epsilon(z)$ was slightly larger than $u_*^3/\kappa z$ in the OBL and decreased gradually throughout the water column (Fig. 1g).

d. *Statistical aspects of* ϵ

For the purpose of statistical analysis, data was grouped according to the two experiments (Table 3). Examination of the data showed a significant difference between the statistics of OR89 night 1 and those of the other datasets. This is probably related to the difference in atmospheric forcing and sea-state conditions during the experiments. For the dataset from OR89 night 1, where the mean profile showed $\epsilon/(u_*^3/\kappa z) \gg 1$, $\epsilon(z)/\bar{\epsilon}$ had a smaller median and a larger average deviation (AD; defined in the caption of Table 3), and $\epsilon/(u_*^3/\kappa z)$ had a larger mean, median, and AD, compared to the datasets for which mean profiles showed $\epsilon/(u_*^3/\kappa z) \sim 1$. Implications of the statistical behavior described above are discussed in section 5.

4. TKE—no surface waves

If the upper boundary of the ocean is treated as a solid surface (e.g., when surface waves are nonexistent or can be neglected), the terms in the momentum and kinetic energy equations describing interactions with the wave field vanish. The equations become those used for a boundary layer over a solid surface, as for the ABL over land, and one expects similar scaling laws to hold for the OBL. The TKE equation for a steady state, neglecting transport terms, results from either Eq. (9) or (17)

$$-\frac{g}{\rho}\overline{w'\rho'} - \overline{w'u'}\frac{\partial \bar{U}}{\partial z} - \epsilon = J_b + P - \epsilon = 0. \quad (18)$$

Here P, the shear production, is the rate of TKE production by the interaction of the turbulence Reynolds stress and the mean shear and is almost always positive. The buoyant production, J_b, is the rate of work done by/against the buoyancy forces and might be either a source/sink of TKE, depending on the sign of the vertical buoyancy flux, $\overline{w'\rho'}$. In the OBL this term is negative (a sink) during daytime heating, while during convective conditions (nighttime, cold air outbreaks) it is positive (a source). The TKE dissipation rate, ϵ, is always positive.

a. *Surface-layer similarity*

In the atmospheric surface layer (ASL) over land (the lower 10% of either the stable or unstable ABL) turbulence fluxes are approximately constant with height (Haugen et al. 1971). Constancy of momentum flux (stress), $\overline{w'u'}$, can be readily obtained from (4) and a steady state. That is,

$$\frac{\partial}{\partial z}\left(\nu\frac{\partial \bar{U}}{\partial z} - \overline{w'u'}\right) = 0, \quad (19)$$

so that

$$\nu\frac{\partial \bar{U}}{\partial z} - \overline{w'u'} = \frac{\tau_0}{\rho_w}. \quad (20)$$

The first term in (20), representing the viscous stress, is important only very close to the surface [O(0.01 m)] and can be neglected farther away, resulting in

$$-\overline{w'u'} = \frac{\tau_0}{\rho_w} = u_*^2. \quad (21)$$

Similarly it can be shown that for steady state the buoyancy (or heat) flux in the SL is constant

$$-\frac{g}{\rho}\overline{w'\rho'} = J_b^0. \quad (22)$$

TABLE 3. Columns 4 and 5 are statistics of $X = \epsilon/\bar{\epsilon}$, the TKE dissipation rate normalized by its mean value for the respective dataset. Columns 6–8 are statistics of $X = \kappa z\epsilon/u_*^3$, the TKE dissipation rate normalized by wind stress scaling. The median is the value X_{med} for which larger and smaller values of X are equally possible. The average deviation (AD) (or mean absolute deviation) for a quantity X is defined by $\text{AD}(x_1 \cdots x_N) = (1/N)\sum_{j=1}^{N} |x_j - \bar{x}|$ and is a more robust estimate of the variability around the mean than the standard deviation (Press et al. 1986).

Experiment	Depth interval (m)	$10^7\bar{\epsilon}$ (m^2 s^{-3})	$\epsilon/\bar{\epsilon}$		$\kappa z\epsilon/u_*^3$		
			Median	AD	Mean	Median	AD
OR89 night 1	0.5–D	247.0	0.12	1.37	6.38	1.72	7.53
OR89 night 2	0.5–D	7.97	0.45	1.00	1.61	0.73	1.51
OR90 daytime	0.5–D	5.35	0.32	1.14	0.31	0.17	0.25
OR90 nighttime	0.5–D	6.02	0.14	1.44	1.83	0.16	2.92
OR90 all data	0.5–D	5.95	0.17	1.41	1.66	0.16	2.62

Since the ASL is approximately a constant-flux layer, its structure is determined by the surface wind stress, τ_0 (or u_*); the surface heat flux, J_q^0; and the buoyancy parameter, g/T (g is the gravitational acceleration and T is a representative ASL temperature). Here J_q^0 and g/T can be combined into the buoyancy flux, $J_b^0 = (g/T)J_q^0/\rho c_p$, where c_p is the specific heat at constant pressure. Since the land surface provides a rigid boundary, the height z above the surface defines the maximal length scale of the large eddies. Normalization of SL variables by the controlling parameters, z, u_*, g/T, and J_q^0 (or J_b^0), and formation of dimensionless groups is defined as SL similarity scaling (or Monin–Obukhov similarity scaling or constant stress-layer scaling). The dimensionless groups formed with these parameters are expected to be universal functions of z/L, where $L = -u_*^3/\kappa J_b^0$ is the Monin–Obukhov length scale.

If SL scaling is applicable, the TKE budget (18) can be nondimensionalized through division by $u_*^3/\kappa z$. With the aid of (21) and (22), we have

$$\frac{z}{L} + \frac{\kappa z}{u_*}\frac{\partial \bar{U}}{\partial z} - \frac{\kappa z}{u_*^3}\epsilon = 0. \tag{23}$$

Then SL similarity theory predicts that the terms in (23) will be universal functions of z/L [note that (23) also assumes stationary and horizontally uniform conditions that are hardly ever met in reality].

Scaling regimes in the stable and unstable ABL are commonly defined by the nondimensional length scales z/D (D is the height of the ABL), z/L (e.g., Nichols and Readings 1979), or by z/D and D/L (Holtslag and Nieuwstadt 1986). Here D/L is a bulk stability parameter describing the overall structure of the ABL, while z/L can be considered a local stability parameter at some specific height z. For small $|D/L|$ (or $|z/L|$), the stratification is close to neutral, while for increasing values the effects of stability become more important. Following Holtslag and Nieuwstadt, the SL scaling regime in the unstable ABL ($L < 0$) is defined for $0.1 > z/D > 0.01$ and $5\text{–}10 > -D/L > 1$. For $0.8 > z/D > 0.1$ and $5\text{–}10 > -D/L > 1$ a near-neutral upper layer (NNUL) is indicated. This layer exists often above the sea (Nichols and Readings 1979), and in addition to D, the SL scaling parameters are also relevant in this regime. In the stable ABL ($L > 0$), SL scaling is considered applicable for $0.1 > z/D > 0$ and $10 > D/L > 0$. The region $1.0 > z/D > 0.1$ and $1 > D/L > 0$ is considered a NNUL. In terms of the local stability parameter z/L, SL scaling in the ABL is found to be generally valid in the range $1 > z/L > -2$ (e.g., Wyngaard 1973).

The stability parameters D/L and z/L depend on the value of L, which, in turn, is completely determined by atmospheric forcing—namely, the surface wind stress and surface buoyancy/heat flux. Since the ASL responds relatively fast to changes in surface forcing, D/L and z/L are generally a suitable measure of stability in the ASL. However, the OBL responds much slower to changes in surface forcing, and D/L and z/L may not always represent the actual stability of the upper OBL (additional processes, such as surface wave activity, might render the comparison between the OBL and the ABL, based on the parameters D/L or z/L, even less applicable). In our opinion, a comparison of background stratification in the upper OBL and in the ASL can be better made using the dimensionless temperature gradient, $\Phi_h \equiv (\kappa z/\theta_*)\bar{\theta}_z$, where $\theta_* = J_q^0/\rho c_p u_*$. The advantage in using Φ_h is that it takes the actual background stratification into account. Examination of our experiments in terms of SL scaling applicability follows and is compared to ASL results.

b. OR89

Following ABL nomenclature, the estimates of z/L (Table 2) classify the OBL as being close to neutral for the two nights of the experiment and SL scaling applicable in the range -0.5 m $> z > -D$ (for comparison, in the ASL $\Phi_h \sim 1$ for $z/L \sim 0$, that is, for neutral stratification). Inspection of Figs. 1a and 1b shows that θ was uniform in the upper 12 m or so of the OBL, supporting the notion of neutral stratification. Comparison of $\epsilon(z)$ to $u_*^3/\kappa z$ shows a clear distinction between the two nights: for night 2, $\epsilon/(u_*^3/\kappa z) \sim 1$ in the upper 10 m or so (Fig. 1b), as expected from SL scaling, while for night 1 ϵ was larger than expected from SL scaling alone (Fig. 1a). To quantify the excess in dissipation over $u_*^3/\kappa z$, we calculated the ratio of the depth-integrated dissipation rate to the depth-integrated wind stress production in the depth interval -0.5 m $> z > -D$, $\int_{-D}^{-0.5} \rho\epsilon dz / \int_{-D}^{-0.5} \rho(u_*^3/\kappa z)dz$. The value of this ratio (Table 2) for night 1 is an order of magnitude larger than that of night 2, reflecting the significant difference between the two nights.

c. OR90

Estimates of z/L (Table 2) classify the OBL as slightly stable during daytime and slightly unstable during nighttime, with SL scaling applicable for -0.5 m $> z > -D$. In this depth range, for day 1 and night 3 (Figs. 1c and 1g, respectively), $\epsilon(z)$ was slightly larger than $u_*^3/\kappa z$ and $\int \rho\epsilon dz / \int \rho(u_*^3/\kappa z)dz \sim 2$ (Table 2), while for night 1, $\epsilon(z)$ was slightly smaller than $u_*^3/\kappa z$ (Fig. 1e). Considering the 95% confidence intervals and that ϵ is determined to within a factor of 2 (Moum et al. 1995), the departure of $\epsilon(z)$ from $u_*^3/\kappa z$ for day 1 and nights 1 and 3 is probably insignificant. For day 2 (Fig. 1d) and night 2 (Fig. 1f), a larger departure, with values of $\epsilon(z)$ smaller than the predicted wind stress scaling, can be noticed.

TABLE 4. Estimates of the rate of energy lost by wind wave breaking, R, calculated from Eqs. (24), (27), and (28); the depth-integrated dissipation rates, $\int \rho\epsilon dz$; and the depth-integrated wind stress production term $\int (\rho u_*^3/\kappa z)dz$ (all units are W m^{-2}). There are three rows of estimates of R. In the first row we have used the wave parameters from R/V *Wecoma*'s ship's officers' log (Table 1). Estimates of R in the second row are based on values of $\bar{T}$ and E as determined from the wind speed, U_{10}, and the formulation suggested by Longuet-Higgins (1969). Values of R in the third row are estimated from the relations between the wave parameters and U_{10} as suggested by Neumann and Pierson (1966). The fourth and fifth rows represent estimates of R using the parameters of the two swells from *Wecoma*'s log (see also text). Values in the left column of the estimate based on Eq. (24) were calculated using $p = 2.4 \times 10^{-4}$, where $\beta = 1.5 \times 10^{-2}$ (Hasselmann et al. 1973) was used, and those in the right column using $p = 13.9 \times 10^{-4}$, where $\beta = 1.9 \times 10^{-2}$ (Forristall 1981) was used. Values in the left column of the estimate based on Eq. (27) were calculated using $f(U_{10})$, the fraction of breaking waves as a function of U_{10}, as observed by Holthuijsen and Herbers (1986) and those in the right column using $f(U_{10})$ as observed by Thorpe and Humphries (1980). Values in the left and right columns of the estimate based on Eq. (28) were calculated using $\gamma = 0.1$ and $\gamma = 1.0$, respectively (Kitaigorodskii 1983). Here $\int \rho\epsilon dz$ was integrated between 0.5 and 13.5 m. For comparison with constant stress-layer scaling, $\int (\rho u_*^3/\kappa z)dz$ was calculated for the same depth interval.

Experiment	Energy lost by breaking, R			$\int \rho\epsilon dz$	$\int (\rho u_*^3/\kappa z)dz$
	Eq. (24)	Eq. (27)	Eq. (28)		
OR89 night 1					
Wecoma's wind waves	(0.075, 0.44)	(1.25, 6.89)	(0.16, 1.56)	0.362	0.033
U_{10} (Longuet-Higgins 1969)	(0.30, 1.72)	(4.96, 27.28)	(0.31, 3.13)		
U_{10} (Neumann and Pierson 1966)	(0.51, 2.94)	(8.47, 46.57)	(0.25, 2.54)		
Swell 1 (H_s = 3.0 m, T = 12 s)	(0.23, 1.31)	(3.76, 20.68)	(0.47, 4.68)		
Swell 2 (H_s = 2.5 m, T = 6 s)	(0.31, 1.81)	(5.22, 28.72)	(0.23, 2.34)		

We note that the relatively large magnitude of L (Table 1), combined with the small OBL depths, resulted in relatively small values of $-D/L$: 0.24 to 0.31 and 0.07 to 0.27 during the nights of OR89 and OR90, respectively (Table 2). In this range convective scaling is considered not applicable and explains why ϵ did not scale with J_b^0. The apparent departures of $\epsilon(z)$ from that expected by SL scaling during our experiments are discussed next.

5. TKE—Effects of surface waves

Because the OBL has a free surface, and hence can support surface waves, we need to consider the range of influences these can have on near-surface turbulence. We should not simply expect the near surface of the ocean to behave as the near surface of the atmosphere over solid boundaries. Surface waves can produce or interact with turbulence in different ways. In section 5a we estimate the energy lost by breaking surface waves to determine if the observed $\epsilon(z)$ profiles are consistent with energetics considerations. Then we develop two new scalings for $\epsilon(z)$ from TKE equations in section 5b, compare scalings to observations in section 5c, and discuss the influence of wave age in section 5d.

a. *Comparison of vertically integrated $\epsilon(z)$ to energy lost from breaking waves*

An estimate of the energy lost by breaking surface waves can be made in three ways. The first estimate is based on Longuet-Higgins' (1969) theoretical–statistical model. According to this model, the rate of energy lost per unit surface area, R, due to wave breaking is

$$R = \frac{Ep}{\bar{T}}, \tag{24}$$

where E is the total wave energy density per unit horizontal area and p is the proportion of wave energy lost per mean wave cycle, $\bar{T}$. The wave spectrum in the equilibrium range, when the limiting form of the wave spectrum is dominated by wave breaking, is given by $S(\omega) = \beta g^2 \omega^{-5}$, where β is a constant and ω is radian frequency (Phillips 1977). Using this wave spectrum the value of p is given (Longuet-Higgins 1969) by

$$p = \exp\left(\frac{-1}{8\beta}\right). \tag{25}$$

Note that p is quite sensitive to the value of the constant β (see also Table 4). For a narrow wave spectrum, E is related to the rms wave amplitude $\bar{a}$ by

$$E = \frac{1}{2}\rho g \bar{a}^2. \tag{26}$$

A second estimate of energy lost by breaking surface waves uses the laboratory observations of Lamarre and Melville (1991) that about 10% (and up to 40%) of the total prebreaking energy can be lost through breaking (see also Rapp and Melville 1990). Combined with field observations of the fraction, $f(U_{10})$, of breaking waves as a function of wind speed at 10-m height (Thorpe and Humphries 1980; Holthuijsen and Herbers 1986), the rate of energy lost per unit surface area due to breaking can be written as

$$R = \frac{0.1 E f(U_{10})}{\bar{T}}. \tag{27}$$

The factor 0.1 in (27) results from the use of Lamarre and Melville's observation that about 10% of a wave's energy can be lost by breaking.

The third estimate of energy lost by breaking surface waves uses the rate of energy transfer from the wind to the waves, which following Kitaigorodskii (1983), is given by

$$W = \gamma \tau_0 \bar{C}, \tag{28}$$

where γ is a coefficient on the order of 0.1–1.0 and $\bar{C} = (g/2\pi)\bar{T}$ is the mean phase speed of the waves. If the wave field is stationary and homogeneous, then the rate of energy lost by breaking should equal the rate of energy input from the wind to the waves; that is, $R = W$.

If most of the wave energy lost by breaking produces turbulence, it might in turn be evidenced in enhanced dissipation rates near the surface. This seems to be supported by laboratory measurements of deep-water breaking waves by Rapp and Melville (1990), who found that more than 90% of the energy lost due to breaking was dissipated within four wave periods. If so, the depth-integrated TKE dissipation rate, $\int \rho \epsilon dz$, in the wave-influenced layer near the surface should be on the order of the rate of energy lost by wave breaking. Assuming that the energy lost is largely due to breaking of wind waves, estimates based on (24), (27), and (28) were made.

Uncertainties in the estimates of R from (24) or (27) may be due to uncertainties in either $\bar{a}$ (since $E \propto \bar{a}^2$) or $\bar{T}$, while uncertainty in the latter is the only wave parameter related uncertainty in estimates of R from (28). Our estimate of the uncertainty in H_s (0.1 m; section 3a) leads to an uncertainty in E of ~25% at a nominal value of $H_s = 1.0$ m for OR89 night 1, where $\bar{a} \sim H_s/2$ (Table 1). Since wave periods from the officers' log are estimated to the nearest full second, we may expect an uncertainty of ~25% in the period of the wind waves of OR89 night 1. For comparison, inverting Holthuijsen and Herbers' (1986) observations of wave steepness, $s \equiv H/(g/2\pi)T^2$, yields $\bar{T} \sim 4.2$ s. This is in good agreement with the value of 4 s from the log book (their observations were made in open sea conditions with winds between 8 and 12 m s^{-1}, which are similar to the conditions that prevailed during OR89, and indicated an average steepness $s = 0.037$). Thus, combining the uncertainties in E (25%) and $\bar{T}$ (25%), the estimates of R from wave parameters are believed to be accurate to within a factor of 2.

Another means of estimating R is solely from the relations between wind and wave parameters for fully developed seas. Two sets of relations were used for our estimates. The first, based on observations and theoretical considerations of the wave height distribution (Longuet-Higgins 1969), suggests that $\bar{T} = 2\pi\bar{C}/g \sim 2\pi U_{10}/g$ and $\bar{a} \sim 0.088 U_{10}^2/g$. The second set of relations, based on the spectral form proposed for fully developed wind seas (Neumann and Pierson 1966), suggests that $\bar{T} = 0.81 \times 2\pi U_{10}/g$ and $H_s = 2.12 \times 10^{-2} U_{10}^2$ (for our estimates we have taken $\bar{a} = H_s/2$).

Estimates of R based on the wave parameters from R/V *Wecoma*'s log and based on the relations between the wind and the waves are presented in Table 4. The estimate of R based on *Wecoma*'s wind waves only (first row of Table 4) appears to be smaller than the other estimates of R (Table 4, rows 2–5). This difference may be the result of estimating R from wind wave parameters only, while swell probably contributed to breaking as well. Relatively good agreement exists between estimates of R from swell parameters and from U_{10} (Table 4). The range in R, as represented by the upper and lower values for each estimate, is a function of the range in the estimates of p (a factor ~6), $f(U_{10})$ (a factor of ~3–6), and γ (a factor of ~10).

All of the independent estimates made for the energy lost by breaking surface waves are much greater than the turbulence energy generated by the wind stress as predicted by SL scaling (the rightmost column in Table 4). These estimates are, however, consistent with the observed vertically integrated turbulence dissipation rate, $\int \rho \epsilon dz$ (Table 4).

b. *Scaling $\epsilon(z)$ in a wave field*

1) IRROTATIONAL WAVES

Because high values of $\epsilon(z)$ were observed deeper than e-folding scales of the wind waves, a possible scenario is that breaking waves (mainly wind waves) form a layer near the surface (on the order of the wind wave height) of enhanced TKE, which in turn is transported downward by the swell. This could be achieved via the term $-\partial(\overline{\tilde{w}\frac{1}{2}u_i'u_i'})/\partial z$ [(9) and (17)], which describes the vertical transport of TKE, $\frac{1}{2}\overline{u_i'u_i'}$, by the wave velocity $\tilde{w}$. At first glance it may seem that this term should vanish due to averaging over the sinusoidal vertical wave velocity, $\tilde{w}$. However, consider the following scenario: during the half cycle when $\tilde{w} > 0$, turbulence near the surface decays with time and diffuses spatially as it cannot be transported upward farther through the sea surface; during the half cycle when $\tilde{w} < 0$, turbulence from the surface will be transported downward while decaying and diffusing. Consequently, $-\partial(\overline{\tilde{w}\frac{1}{2}u_i'u_i'})/\partial z$, must be positive on average. That is, away from the surface the magnitude of $\overline{\tilde{w}\frac{1}{2}u_i'u_i'}$ must decrease due to the combined effects of exponential depth decay of $\tilde{w}$ and the decay and spreading of TKE as it is transported downward.

If a surface layer, with thickness of $O(k^{-1})$, is governed by wave–turbulence interactions such that the main local balance is between $-\partial(\overline{\tilde{w}\frac{1}{2}u_i'u_i'})/\partial z$ and the TKE dissipation rate, then

$$\epsilon(z) \sim -\frac{\partial}{\partial z}\left(\overline{\tilde{w}\frac{1}{2}u_i'u_i'}\right)$$

$$\sim -\frac{\partial}{\partial z}\left[\overline{\omega a \exp(kz)\sin(kx-\omega t)\frac{1}{2}u_i'u_i'}\right], \quad (29)$$

where ω and a are the radian frequency and amplitude, respectively, and $\tilde{w} = \omega a \sin(kx - \omega t)\exp(kz)$. Although the depth decay of turbulence (represented by $\frac{1}{2}\overline{u_i'u_i'}$) is not known, the vertical gradient of $\overline{\tilde{w}\frac{1}{2}u_i'u_i'}$ will decay with depth at least as fast as $\exp(kz)$, due to the decay of the vertical wave velocity $\tilde{w}$ alone.

An upper bound on $\epsilon(z)$ in the wave-dominated surface layer can now be found. Assuming, for simplicity of differentiation, a depth-independent (or in turn a depth-averaged) correlation coefficient, r, between $\tilde{w}$ and $u_i'u_i'$, and taking $\frac{1}{2}\overline{u_i'u_i'} \sim \frac{3}{2}u_{\text{rms}}^2 \sim \frac{3}{2}(0.02C)^2$ as an upper bound on the TKE (Rapp and Melville 1990), we find from (29)

$$\epsilon(z) \leqslant a\frac{1}{\pi}g^{1/2}k^{3/2}r\frac{3}{2}(0.02C)^2\exp(kz), \quad (30)$$

where $\omega^2 = kg$ and averaging is performed over half the cycle of downward transport, that is, when $\tilde{w} < 0$. It should be noted that if breaking of wind waves is the main source for TKE, the phase speed C of the wind waves must be used to estimate the TKE, $\frac{1}{2}\overline{u_i'u_i'}$, in (30), while other wave parameters are derived from the swell.

2) Rotational waves

If on the other hand the wave field is not truly irrotational, as reported by some investigators (section 2c), the resulting wave stresses may indirectly enhance turbulence in the wave-influenced layer near the surface. Assuming steady state and neglecting molecular diffusion, the KE equation for the mean flow (15) reduces to

$$-\overline{w'u'} - \overline{\tilde{w}\tilde{u}} = \text{const} = \frac{\tau_0}{\rho}. \quad (31)$$

Cheung and Street (1988) found that $-\overline{\tilde{w}\tilde{u}}$ and $-\overline{\tilde{w}\tilde{u}}\partial\bar{U}/\partial z$ were generally negative, decaying rapidly with depth. Thus, energy is transferred from the wave field to the mean field via the term $\overline{\tilde{w}\tilde{u}}\partial\bar{U}/\partial z$, which appears in (15) and (16) with opposite signs. If, in the wave-dominated layer near the surface, the wave stresses are much larger than the surface wind stress (e.g., Shonting 1964; Cavaleri et al. 1978) such that $\overline{\tilde{w}\tilde{u}} \gg \tau_0/\rho$, then, to satisfy the balance in (31), one arrives at

$$-\overline{w'u'} \sim \overline{\tilde{w}\tilde{u}} \gg \tau_0/\rho. \quad (32)$$

This balance, depicted schematically in Fig. 2, does not violate the continuity of tangential stress across the air–water interface, but rather allows for much larger respective wave and turbulence stress terms than would be predicted from an estimate τ_0/ρ derived from surface winds.

If the wave stress is simply a result of $\tilde{u}$ and $\tilde{w}$ being out of quadrature (e.g., Yefimov and Khristoforov 1969; Cavaleri et al. 1978), the orbital wave velocities can be defined as follows:

$$\tilde{u} = a\omega\cos(kx - \omega t)\exp(kz), \quad (33a)$$

$$\tilde{w} = a\omega\sin(kx - \omega t + \phi)\exp(kz), \quad (33b)$$

where ϕ is the phase shift from quadrature (although ϕ may be depth dependent, we assume for simplicity that ϕ is a constant considered here as a representative value for the layer influenced by the wave stress). From (33a) and (33b) and with the aid of trigonometric identities

$$\overline{\tilde{w}\tilde{u}} \approx \frac{1}{2}a^2gk\exp(2kz)\sin\phi, \quad (34)$$

where $\omega^2 = gk$. An exponential decay of mean wave stress was observed by Cheung (1985) for wind-ruffled mechanically generated waves, and similar results were reported by Bliven et al. (1984), for both paddle-generated waves and paddle-generated waves with an imposed wind stress. Assuming that the main balance in

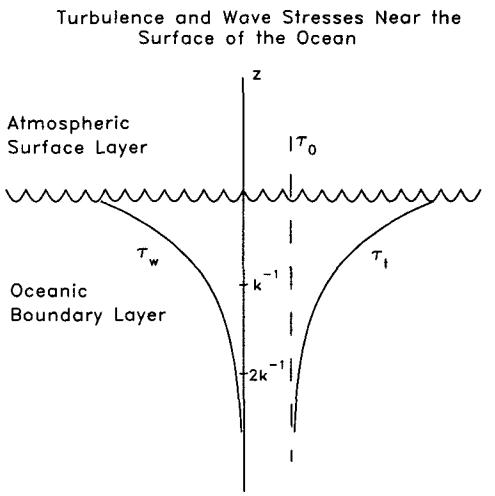

FIG. 2. Schematic depicting the stress balance, $\tau_t + \tau_w = \tau_0$, near the surface of the ocean allowing for wave-generated stresses [see section 5b, Eq. (31)]. Here $\tau_t = -\rho_w\overline{w'u'}$ is the turbulence Reynolds stress, $\tau_w = -\rho_w\overline{\tilde{w}\tilde{u}}$ is the wave stress, and $\tau_0 = \rho_w C_D U_{10}^2$ is the wind stress calculated using U_{10}, the wind speed at 10-m height, and C_D is the drag coefficient. This balance does not violate the requirement of stress continuity across the air–sea interface. If this balance exists and can be modeled as in (34), then the depth decay of τ_t, or for that matter of τ_w, is exponential with a decay constant of $2k$ (the vertical scale is exaggerated to highlight the exponential depth decay).

(17) is between the TKE dissipation rate, ϵ, and the shear production, $-\overline{w'u'}\partial\bar{U}/\partial z$, and using (32) and (34), results in

$$\epsilon = -\overline{w'u'}\frac{\partial \bar{U}}{\partial z} \approx \frac{1}{2}a^2 gk \exp(2kz)\sin\phi \frac{\partial \bar{U}}{\partial z}. \quad (35)$$

Although the two mechanisms proposed above to explain the observed high ϵ values in the near surface layer—namely, the transport of TKE by swell and the indirect production of TKE via wave stresses—are physically different, both processes might affect turbulence and mixing in a surface layer of $O(k^{-1})$.

An additional wave–turbulence interaction term that needs to be considered is $-\overline{u_i' u_j'}\partial\tilde{u}_i/\partial x_j$ [Eqs. (9) and (17)], which describes TKE production by the interaction of the turbulence Reynolds stress and the periodic wave shear. This type of interaction might be important for turbulence with timescales $T_t \ll T$, that is, much shorter than the wave period, T, such that the turbulence perceives the wave field as a slowly varying shear flow (Kitaigorodskii and Lumley 1983). If the turbulence velocity scale is u_t and the length scale l_t, then $l_t/u_t \ll T$. Using the empirical relation, $\epsilon \approx u_t^3/l_t$, we arrive at the condition for the turbulence velocity, $u_t \ll (T\epsilon)^{1/2}$. For representative values of $\epsilon \sim 10^{-5}$ m^2 s^{-3}, observed at a depth of about 5 m during OR89 night 1, and $T \sim 10$ s we get $u_t \ll 0.01$ m s^{-1}. This velocity scale is even smaller than the surface friction velocity for OR89 night 1 ($u_* = 0.016$ m s^{-1}), and is too small and inconsistent with the increased turbulence levels we observed near the surface. Moreover, an estimate of the turbulence length scale, based on the above considerations, results in $l_t \ll 0.1$ m. The relatively short turbulence length scale required for this mechanism to be effective probably renders it unimportant in vertical mixing of the OBL, compared to the larger eddies that have sizes on the order of meters.

c. *Comparison of predicted scalings to our observations*

Simple exponential forms, $\epsilon(z) = \epsilon_0 \exp(\alpha z)$, were fit to the observed dissipation rates in the upper part of the OBL (Fig. 3). The observations reveal a change in slope of $\epsilon(z)$ at a depth of ~6 m, with a more rapid depth decay in the upper 6 m. Within the context of our wave-based scalings, one interpretation is that the upper 6 m is dominated by wind waves; whereas, below 6 m, the dominant effect is the longer wavelength swell. The exponential fit to $\epsilon(z)$ was divided into two separate depth intervals (Fig. 3), resulting in $\alpha_1 = 0.66$ m^{-1} and $\alpha_2 = 0.18$ m^{-1} for the depth intervals of 1.5–5.5 m and 5.5–14.5 m, respectively. The surface intercept value, ϵ_0, for the two fits resulted in 2.9×10^{-4} and 2.0×10^{-5} m^2 s^{-3}, respectively.

If dissipation locally balances the downward transport by swell of enhanced surface turbulence produced by wind wave breaking [Eq. (31)], then vertically integrating $\epsilon(z) = \epsilon_0 \exp(\alpha z)$ to the surface should result in a value consistent with the energy lost by wave breaking. Vertical integration results in values of 0.45 and 0.11 W m^{-2} for the fits in the depth intervals of 1.5–5.5 m and 5.5–14.5 m, respectively. Both values are similar to that obtained by integrating the observed $\epsilon(z)$ (Table 4) and are consistent with the estimates of the rate of energy lost by wind wave breaking in Table 4.

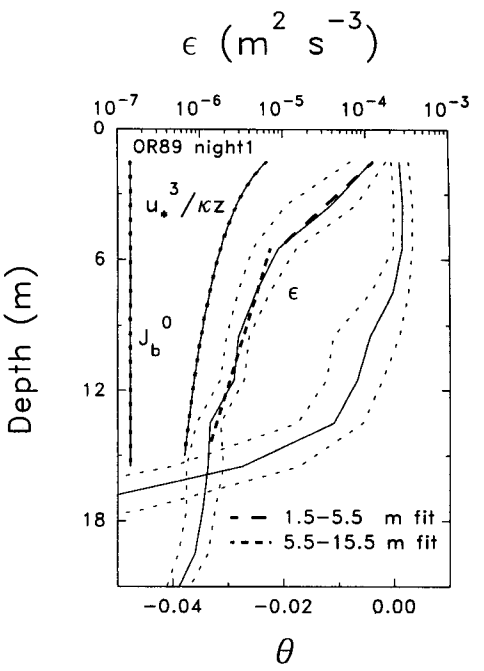

FIG. 3. Fit of the form $\epsilon(z) = \epsilon_0 \exp(\alpha z)$ to the estimated values of ϵ in the upper part of the OBL. For OR89 night 1, a fit in the depth range 1.5–5.5 m (long dashes) results in $\epsilon_0 = 2.9 \times 10^{-4}$ m^2 s^{-3} and $\alpha = 0.66$ m^{-1}, and a fit in the depth range 5.5–14.5 m (short dashes) results in $\epsilon_0 = 2.0 \times 10^{-5}$ m^2 s^{-3} and $\alpha = 0.18$ m^{-1}. Note that down to the base of the OBL (~13 m) $\epsilon(z)$ is larger than predicted by constant stress-layer scaling.

We first consider the mechanism described by (29) and (30), by which TKE generated by breaking wind waves is transported downward by the swell. The depth decay of $\epsilon(z)$ is dictated by that of the orbital velocity of the swell; if the turbulence also undergoes significant diffusion and dissipation over half a wave cycle, then the vertical decay rate will be greater than (30). If in this case downward transport of turbulence is dominated by wind wave transport in the upper part and swell transport in the lower part, then $k_w = \alpha_1 = 0.66$ m^{-1} and $k_s = \alpha_2 = 0.18$ m^{-1}, where k_w and k_s are the wind wave and swell wavenumbers, respectively. These wavenumbers correspond, respectively, to $\lambda_w = 9.5$ m and $\lambda_s = 34.9$ m or to $T_w = 2.5$ s and $T_s = 4.7$ s, compared to the ship's officer's log estimates of $T_w = 4$ s and $T_s = 6$ s (for the shorter of the two swells observed).

Since (30) invokes a correlation coefficient, r, of unknown magnitude, it is important to demonstrate that r need not be large for (30) to be an effective mechanism. An estimate of r_0 (r at $z = 0$) can be made by vertically integrating (29) and evaluating at $z = 0$. For this purpose the TKE, $\frac{1}{2}\overline{u_i'u_i'}$, is estimated as $\sim\frac{3}{2}u_{\text{rms}}^2$ with $u_{\text{rms}} \sim 0.02C_w$ (Rapp and Melville 1990), where C_w is the phase speed of breaking wind waves calculated using a period of $\bar{T}_w = 4.0$ s. The first estimate, assuming that in the upper part the downward transport of turbulence is dominated by wind wave transport, results in $r_0 \sim 0.05$ (we used $k = k_w = 0.66$ m^{-1}, $a_w = 0.5$ m^{-1}, and $\epsilon_0 = 2.9 \times 10^{-4}$ m^2 s^{-3}). If, on the other hand, we assume a downward transport by swell, we find $r_0 \sim 0.01$ (using $k = k_s = 0.18$ m^{-1}, $a_s = 1.2$ m^{-1}, and $\epsilon_0 = 2.0 \times 10^{-5}$ m^2 s^{-3}). Even if we use $u_{\text{rms}} \sim 0.005C_w$, the value of the rms turbulence velocity observed by Rapp and Melville (1990) 60 wave periods after breaking, we find $r_0 \sim 0.75$ and $r_0 \sim 0.16$, for the two different estimates above, which is still less than 1.

The velocity scale, u_t, for turbulence resulting from wave breaking is estimated next and compared to laboratory observations. Assuming an eddy length scale $l_t \sim H$, where H is the height of the breaking waves, and using the relation $\epsilon = u_t^3/l_t$, with $\epsilon \sim \epsilon_0$, where ϵ_0 is the surface intercept value of the exponential fit, we obtain $u_t = 0.066$ m s^{-1} (using $\epsilon_0 = 2.9 \times 10^{-4}$ m^2 s^{-3}). Expressed in terms of the phase velocity, C_w, of the wind waves, this is equivalent to $u_t = 0.011C_w$. This is consistent with the range of 0.005–$0.02C_w$ of rms turbulence velocities resulting from wave breaking observed by Rapp and Melville (1990). For comparison, if near the surface $u_t \sim u_*$, we find $u_t \sim 0.016$ m s^{-1}. The latter value of u_t is smaller by a factor of 4, compared with that estimated above, resulting in an underestimate of ϵ by almost two orders of magnitude.

Next we consider the mechanism described by (35), by which wave-induced shear stresses in a rotational wave field interact with the mean flow and the turbulence to affect a depth decay rate of $\epsilon(z)$ determined by the decay rate of the wave stress (34). In this case, $\epsilon(z) \propto \exp(2kz)$ (or $\alpha = 2k$ for comparison to the data). Assuming that the change in slope of the exponential in Fig. 3 is due to dominance of wind waves near the surface and swell deeper, we find $k_w = \alpha_1/2 = 0.33$ m^{-1} and $k_s = \alpha_2/2 = 0.09$ m^{-1} corresponding to $\lambda_w = 19.0$ m ($T_w = 3.5$ s) and $\lambda_s = 69.8$ m ($T_s = 6.7$ s), respectively. A lower limit on $\sin\phi$, in the wave stress dominated surface layer, can be estimated from the balance in (35) (see the appendix) as

$$\sin\phi > \frac{2\int_h^0 \epsilon dz}{a^2 gk\bar{U}(0)}. \tag{36}$$

Our estimate from Fig. 3 results in $\sin\phi > 0.11$ ($\phi > 6^0$), where we used the wind wave amplitude $a_w \sim 0.5$ m (Table 1), $k_w g = (\alpha_1/2)g \sim 3.2$ (rad s^{-1})^2, $\int_{-5.5}^0 \epsilon dz \sim 4.4 \times 10^{-4}$ m^3 s^{-3} (calculated from the parameters of the exponential fit in the 1.5–5.5-m depth interval), and assumed a mean surface current $\bar{U}(0) = 0.01$ m s^{-1}. A similar estimate, with a swell amplitude of $a_s \sim 1.2$ m (Table 1), $k_s g = (\alpha_2/2)g \sim 0.9$ (rad s^{-1})^2, $\int_{-14.5}^0 \epsilon dz \sim 1.1 \times 10^{-4}$ m^3 s^{-3} (calculated from the parameters of the fit in the 5.5–14.5-m depth interval), and $\bar{U}(0) = 0.01$ m s^{-1}, results in $\sin\phi > 0.018$ ($\phi > 1^0$). In other words, to explain the observed TKE dissipation rates near the surface, only a small departure from quadrature (on the order of a few degrees) is needed. For comparison; Shonting (1970), Yefimov and Khristoforov (1969), and Cavaleri et al. (1978) have reported phase shifts from quadrature as large as 20^0–30^0 in the upper few meters of the OBL.

d. *Influence of wave age on wave–turbulence interaction*

Compared to the equilibrium phase, when the rate of energy lost by wave breaking balances the energy input by the wind, during the development phase of a wave field a relatively larger part of the wind energy might go into the wave field than is lost by wave breaking. Thus, during the growing phase of the wind wave field, energy and momentum transfer from the wind to the OBL below the wind waves may be less efficient and u_*, inferred from the wind speed at 10 m, may be an overestimate of the turbulence velocity scale and result in overestimates of ϵ in the constant stress-layer formulation. This argument provides a potential explanation for the lower than predicted ϵ values we observed during OR90 day 2 (Fig. 1d), when winds stabilized after a period of rising, and during OR90 night 1 (Fig. 1e), when winds were in the last phase of a rising trend.

Although this explanation seems plausible, it cannot explain the lower values of ϵ than predicted by $u_*^3/\kappa z$ observed during night 2 of OR90 (Fig. 1f), when winds decreased during the second half of the night.

e. *Uncertainties in the determination of the depth dependence of* ϵ

Our data analysis is referenced in the vertical to the sea surface, which undulates due to the presence of surface waves. However, our theoretical analysis is relative to a fixed Eulerian reference frame. This leads to uncertainties in comparing theory and observation. In particular, one result would be a smearing of ϵ in the vertical coordinate. For a given uncertainty in depth, δz, the corresponding uncertainty in ϵ of the form $\epsilon = \epsilon_0 e^{-kz}$ is $\delta\epsilon = -k \cdot \delta z \cdot \epsilon$. This is larger for short

waves, and using the values from our example in Fig. 3 ($k \approx 0.7$ m^{-1}, and an uncertainty in depth of the order of the swell amplitude ~ 1.5 m) gives $\delta\epsilon \approx \epsilon$, or about a factor of 2. As this is smaller than the confidence limits in Fig. 3 that represent the observed variability, we do not consider this a limiting factor in comparing theory and observation. Another consideration is that our profiling, which was random in relation to the wave phase, resulted in data samples with relatively even distribution of the sea surface relative to the quiescent $z = 0$ level. That is, there is no reason to expect an imposed bias in the observations.

Our suggestion of an exponential depth decay of $\epsilon(z)$ due to surface wave–turbulence interactions is consistent with the observed wave parameters. For example, the wave periods deduced from wavenumbers resulting from the exponential fit to $\epsilon(z)$ compare favorably with the observed periods. Similarly, assuming our proposed scaling for wave–turbulence interactions, neither large correlation coefficients [e.g., $r \sim 0.01$ in Eq. (30)] nor large departures from irotationality [e.g., ϕ on the order of several degrees in Eq. (35)] need to be invoked to explain the observed values $\epsilon(z)$. This does not confirm that wave–turbulence interactions are responsible for the observed depth dependence. Other things happen in the upper ocean and other fits can be made to the data. The theory remains to be more rigorously tested.

6. Synopsis of recent near-surface observations of ϵ

Some recent experimental studies in the aquatic near-surface zone showed ϵ to follow the predicted SL scaling, while others showed dissipation rates to be much larger. Vertical profiles of high-frequency temperature fluctuations were made by Dillon et al. (1981) in the neutrally stratified near-surface layer of a reservoir, with no remotely generated swell, when winds averaged 4.8 m s^{-1}, surface wave heights were 0.1–0.2 m, and occasional whitecapping was observed. Dissipation rates, estimated from the high-frequency temperature profiles, followed $u_*^3/\kappa z$ rather well between 1-m depth and the base of the BL at about 6 m. However, from the surface to a depth of 1 m, turbulence was so intense that dissipation rates could not be resolved reliably. From data collected in a reservoir, when winds were between 2 and 6.5 m s^{-1}, Imberger (1985) suggested that ϵ followed the predicted z^{-1} decay in the upper 30% of the BL, although with a great deal of scatter. Soloviev et al. (1988, 1989), using a tethered free-rising profiler, made velocity microstructure measurements in the upper OBL during night under relatively calm conditions of wind speeds of 1.9 to 6.5 m s^{-1} and wind waves ranging from ripples to 0.5 m in height and periods up to 4 s and swells 0.5–1.0 m in height and periods of 6–7 s. Dissipation rates, estimated from the vertical component of the turbulence velocity fluctuations, were near or just above $u_*^3/\kappa z$ in the depth range of a few centimeters to about 5 m. Convection was found to play an appreciable role only at depths greater than 5 m. Lombardo and Gregg (1989) demonstrated that, for a bulk stability of $1 > -D/L$, ϵ followed wind stress scaling, with a mean value of $\epsilon/(u_*^3/\kappa z)$ of 1.76, in the depth range of $0.8 > -z/L > 0.15$ and $z > -5$ m.

In direct contrast to the results described above, an increasing body of observations in the aquatic near-surface zone shows that ϵ is often much larger than predicted by SL and/or convective scaling. Kitaigorodskii et al. (1983) measured TKE dissipation rates beneath wind waves in Lake Ontario that were two orders of magnitude larger than $u_*^3/\kappa z$. Moreover, the depth dependence of ϵ was inconsistent with pure shear-produced turbulence, and the rms turbulence velocities had a strong dependence on wave energy that could not be explained by SL similarity theory. Kitaigorodskii and Lumley (1983) explored possible wave–turbulence interactions, suggesting that the term $-\partial(\overline{w'\frac{1}{2}\tilde{u}_i\tilde{u}_i})/\partial z$, which appears in (18.1) for the TKE of an irrotational wave field, might explain the enhanced dissipation rates they observed. They argue that one of the mechanisms that can explain why w' and $\tilde{u}_i\tilde{u}_i$ may be correlated is associated with the process of wave breaking in a random surface wave field. Breaking events increase the probability that the vertical turbulence velocity, w', is directed downward, leading to a downward surface energy flux. An exponential fit to one dataset (Kitaigorodskii et al. 1983) showed ϵ to be approximated very well by an exponential in z with a decay constant of $3k_p$, where k_p is the wavenumber of the peak of the wave spectrum. This behavior of ϵ appeared to be consistent with the parameterization of $\overline{w'\tilde{u}_i\tilde{u}_i}$ suggested by Kitaigorodskii and Lumley (1983).

Dissipation rates in a strongly convecting OBL (Gregg 1987), showed that although convective similarity scaling described ϵ well in the convective regime deep in the OBL, it failed closer to the surface. Intense near-surface dissipation rates, with averages several decades larger than the sum of J_b^0 and $u_*^3/\kappa z$, extended as deep as 30 m. Below this depth ϵ decreased abruptly to levels approximating J_b^0. Gregg suggested that at least one of the following mechanisms, convective plumes, breaking surface waves, or Langmuir cells, were responsible for producing the intense dissipation rates. Although we cannot ignore the possibility of contribution from Langmuir cells, our observations do not permit an estimate of their effect on the elevated dissipation levels we observed.

From data collected in the northeast Pacific throughout a week and a half of intermittently stormy weather, and over a wide range of wind forcing, Gargett (1989) presented vertical profiles of ϵ near the surface that consistently showed a depth dependence closer to

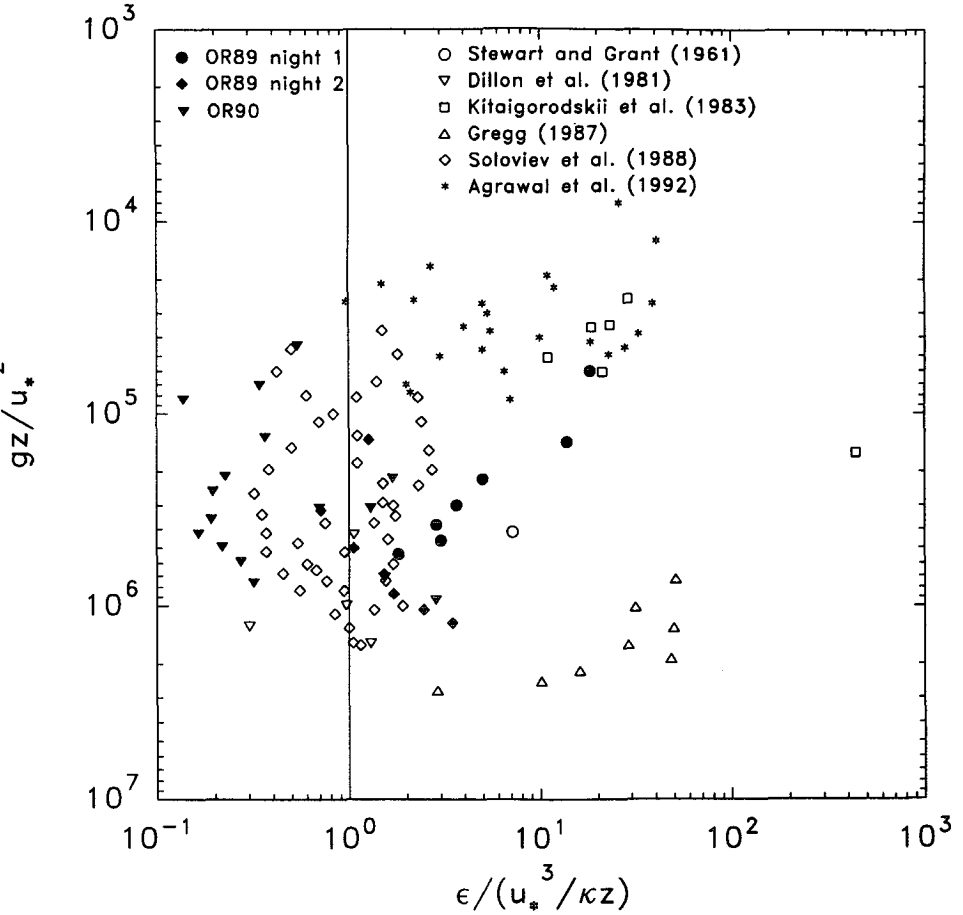

FIG. 4. Dimensionless dissipation rate, $\epsilon/(u_*^3/\kappa z)$, as a function of dimensionless depth, gz/u_*^2. The constant stress layer is represented by the vertical line $\epsilon/(u_*^3/\kappa z) = 1$. Datasets are labeled on the plot with their reference.

z^{-4} than the predicted z^{-1}. However, during the last day of the experiment, when wind speed and sea state decreased, ϵ showed an approximate z^{-1} dependence. Gargett stated that "although fragmentary data suggest that there may be times when the OBL can be described by a constant-stress layer, unfortunately these times may not coincide with the times when the bulk of the stress-driven air–sea transport occurs."

Osborn et al. (1992) reported results from measurements near the ocean surface during weakly convective conditions, mean winds of 5–9 m s^{-1} and waves of 4-s period, using submarine-mounted turbulence probes and sonars. They found values of ϵ in excess of 10 times those expected from SL and convective scaling and which were closely related to acoustically detected bubble clouds generated by breaking waves.

Dissipation rates from data acquired by three different types of velocimeters during the Water–Air Vertical Exchange Study (WAVES) in Lake Ontario (Agrawal et al. 1992), showed ϵ to be highly intermittent. The background level of ϵ was close to values predicted by SL scaling; however, a fairly large number of dissipation estimates exceeded $u_*^3/\kappa z$ by more than an order of magnitude. The mode of the distribution of ϵ, which was approximately the value expected from SL scaling, corresponded to 1/5 of the mean. Agrawal et al. (1992) suggest that since turbulence production by wave breaking is highly intermittent, profiling devices, which traverse the wave breaking zone rapidly (a few seconds at most), will tend to underestimate the mean dissipation rate.

To summarize the comparison of ϵ estimates from our studies and those discussed above, we plotted (Fig. 4) the dissipation rates scaled by $u_*^3/\kappa z$ versus the depth scaled by u_*^2/g, in a manner consistent with the presentation of Soloviev et al. (1988). Vertically integrated dissipation rates in the OBL, $\epsilon_I = \int_{-D}^{0} \epsilon dz$, from different experiments, are compared to the wind power, $E_{10} = \tau_0 U_{10}$, in Fig. 5. The solid line, adapted from an empirical fit by Oakey and Elliott (1982), estimates that about 1% of E_{10} is dissipated in the OBL. Although this estimate seems to work well for OBLs

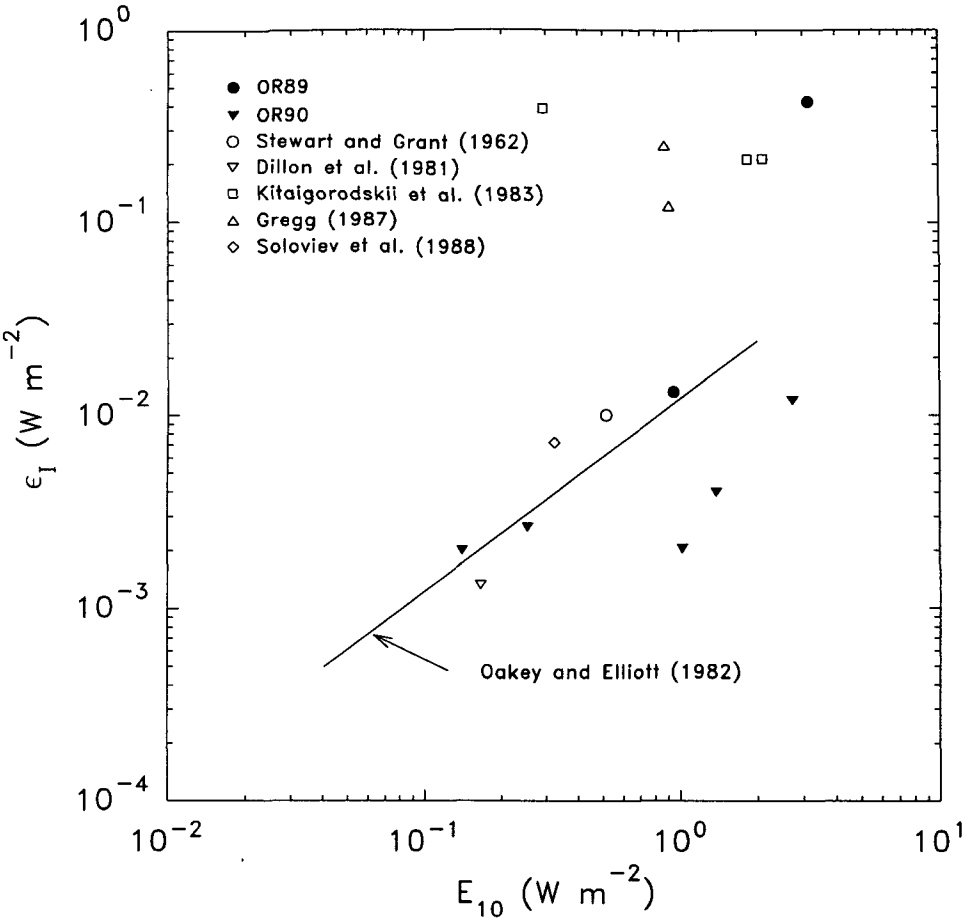

FIG. 5. Depth-integrated dissipation rate in the OBL, ϵ_I, vs wind power at 10-m height, $E_{10} = \tau_0 U_{10}$. Datasets are labeled according to their source. The solid line is adapted from Oakey and Elliott (1982) and indicates 1% of E_{10} dissipated in the ML. This prediction seems to work well for cases where ϵ scales as $u_*^3/\kappa z$; however, a number of datasets have dissipation rates on the order of 10% of E_{10}. Although the number of these cases may be relatively small, they need to be taken into account since average values of ϵ in the OBL may be completely dominated by the higher values.

obeying SL scaling, quite a few of the data lie above this line with representative values of ϵ_I on the order of 10% of E_{10}. In this context it is of interest to note that Richman and Garrett (1977), using field and laboratory experiments in combination with a model of momentum and energy transfer by the wind to the ocean, estimated an input to the ocean of 4%–9% of E_{10} (including the energy that goes into wave breaking). Figures 4 and 5 support the conclusion that we cannot ignore the many cases where simple SL scaling grossly underestimates the observed TKE dissipation rates in the near-surface layer. Even if enhanced dissipation levels prove to be relatively scarce, the physics needs to be resolved since such events frequently dominate the overall average dissipation rate.

7. Conclusions

Measurements of turbulence in the OBL were made by profiling upward through the sea surface with a microstructure profiler. These covered a wide range of atmospheric forcing and sea states. Some of our experiments showed that $\epsilon \sim u_*^3/\kappa z$. However, others showed dissipation rates larger by up to an order of magnitude or more than predicted for TKE produced solely by surface wind stress and buoyancy flux. This suggests enhanced mixing in the near-surface layer of the ocean when compared to the ASL. The presence of swell in conjunction with wind waves, and the fact that the depth dependence of $\epsilon(z)$ was close to exponential with a decay rate on the order of the inverse wavenumber of the waves, suggest wave-related turbulence in the upper part of the OBL.

Kitaigorodskii and Lumley (1983) have suggested that wave–turbulence interaction may occur via the turbulent transport of wave energy, represented by the term $-\partial(\overline{w' \tfrac{1}{2}\tilde{u}_i\tilde{u}_i})/\partial z$. In this paper we propose two new scenarios for the enhanced dissipation rates:

(i) As a result of surface wave breaking, high levels of TKE are produced in a thin surface layer with thickness of the order of the height of the breaking waves. Turbulence is then transported downward by the motion of the swell, while decaying with time and diffusing spatially. This causes the divergence term $-\partial(\tilde{w}\frac{1}{2}\overline{u_i'u_i'})/\partial z$ to assume positive values. If this divergence term is balanced by the TKE dissipation rate, an upper bound $\epsilon(z) < 3 \times 10^{-6} a_s g^{1/2} k_s^{3/2} C_w^2 \exp(k_s z)$ is found, where the exponential depth decay is due to the vertical swell velocity. The actual depth decay of ϵ will be greater than $\exp(k_s z)$ if spatial diffusion and dissipation of turbulence are significant over a wave period; and in the stable case also due to destruction of TKE by buoyancy forces. Independent estimates of the energy lost by breaking surface waves are consistent with the vertically integrated dissipation rates.

(ii) If the wave field is rotational, as has been suggested by many studies, an additional mechanism of TKE production via wave stresses is possible. Kinetic energy, transferred from the wave field to the mean field via the wave production term, $-\tilde{w}\tilde{u}\partial\bar{U}/\partial z$, can in turn be drawn from the mean field by turbulence via the turbulence production term, $-\overline{w'u'}\partial\bar{U}/\partial z$. The scaling $\epsilon \approx \frac{1}{2}a^2 gk \exp(2kz) \sin\phi \partial\bar{U}/\partial z$, results from a balance between the turbulence Reynolds stress, $-\overline{w'u'}$, and the wave stress, $\tilde{w}\tilde{u}$. Only a small departure from quadrature [$\phi \sim O(1^0)$ on average] is needed to account for the enhanced levels of ϵ we observed.

Although physically different, both processes may affect the near-surface layer to a depth on the order of k^{-1} (some tens of meters for a long swell). Beneath this layer either SL or convective similarity scalings, or a combination of the two, may be more appropriate.

Due to the limitations of vertical profiling, which are at best snapshots of the variables we measure in the water column, and because of the intermittent nature of turbulence, more deterministic results will need more comprehensive datasets. It is for future work to combine vertical with horizontal profiling or moored measurements, under a variety of sea states, to test the hypothetical mechanisms suggested here and to determine the conditions for which different scaling laws for turbulence hold true.

Acknowledgments. We are grateful to the captain and crew of the R/V *Wecoma* for their efforts during the experimental phase of this study. Long and helpful discussions with Dave Hebert over the course of this work and comments on an earlier version of this paper by Laurie Padman are acknowledged. The authors would also like to thank the reviewers for their constructive and helpful comments. This work was funded by the National Science Foundation (OCE-8608256 and OCE-8716719) and the Office of Naval Research (N00014-89J3211). A. A. was also supported by a personal grant from the Gerson Meerbaum Foundation for Oceanography, the Hebrew University of Jerusalem, Israel.

APPENDIX

A Lower Limit on the Phase Shift from Quadrature of a Rotational Wave Field

Vertical integration of (35) from h, the bottom of the layer influenced by wave stresses, to the surface, results in

$$\int_h^0 \epsilon dz = \int_h^0 -\overline{w'u'}\frac{\partial\bar{U}}{\partial z}dz \approx \int_h^0 \frac{1}{2}a^2 gk \exp(2kz)\sin\phi \frac{\partial\bar{U}}{\partial z}dz, \quad \text{(A1)}$$

assuming $\sin\phi$ to be constant, yields

$$\sin\phi \approx \frac{2\int_h^0 \epsilon dz}{\int_h^0 a^2 gk \exp(2kz)\frac{\partial\bar{U}}{\partial z}dz}, \quad \text{(A2)}$$

but

$$\frac{\partial}{\partial z}[\exp(2kz)\bar{U}] = \exp(2kz)\frac{\partial\bar{U}}{\partial z} + 2k\exp(2kz)\bar{U}, \quad \text{(A3)}$$

so that

$$\exp(2kz)\frac{\partial\bar{U}}{\partial z} = \frac{\partial}{\partial z}[\exp(2kz)\bar{U}] - 2k\exp(2kz)\bar{U} < \frac{\partial}{\partial z}[\exp(2kz)\bar{U}], \quad \text{(A4)}$$

since $2k\exp(2kz)\bar{U} > 0$.
Hence

$$\int_h^0 \exp(2kz)\frac{\partial\bar{U}}{\partial z}dz < \int_h^0 \frac{\partial}{\partial z}[\exp(2kz)\bar{U}]dz = \exp(2kz)\bar{U}|_h^0 = \bar{U}(0) - \exp(2kh)\bar{U}(h) < \bar{U}(0), \quad \text{(A5)}$$

and substitution of (A5) in (A2) results in a lower limit on ϕ given by

$$\sin\phi > \frac{2\int_h^0 \epsilon dz}{a^2 gk\bar{U}(0)}. \quad \text{(A6)}$$

REFERENCES

Agrawal, Y. C., E. A. Terray, M. A. Donelan, P. A. Hwang, A. J. Williams III, W. M. Drennan, K. K. Kahma, and S. A. Kitaigorodskii, 1992: Enhanced dissipation of kinetic energy beneath surface waves. *Nature,* **359,** 219–220.

Anis, A., and J. N. Moum, 1992: The superadiabatic surface layer of the ocean during convection. *J. Phys. Oceanogr.,* **22,** 1221–1227.

Benilov, A. Yu., 1973: Generation of ocean turbulence by surface waves. *Izv. Akad. Nauk. SSSR, Atmos. Ocean Phys.,* **9,** 160–164.

Bliven, L. V., N. E. Huang, and S. R. Long, 1984: A laboratory study of the velocity field below surface gravity waves. *Gas Transfer at Water Surfaces,* W. Brutseart and G. H. Jirka, Eds., Reidel, 181–190.

Bowden, K. F., 1950: The effect of eddy viscosity on ocean waves. *Philos. Mag.,* **41,** 907–917.

Cavaleri, L., and S. Zecchetto, 1985: Reynolds stresses. *The Ocean Surface,* Y. Toba and H. Mitsuyasu, Eds., Reidel, 443–448.

——, J. W. Ewing, and N. D. Smith, 1978: Measurements of the pressure and velocity field below surface waves. *Turbulent Fluxes through the Sea Surface, Wave Dynamics, and Prediction,* A. Favre and K. Hasselmann, Eds., Plenum, 257–272.

Cheung, T. K., 1985: A study of the turbulent layer in the water at an air–water interface. Tech. Rep. No. 287, Department of Civil Engineering, Stanford University, 260 pp.

——, and R. L. Street, 1988: The turbulent layer in the water at an air–water interface. *J. Fluid Mech.,* **194,** 133–151.

Churchill, J. H., and G. T. Csanady, 1983: Near-surface measurements of quasi-Lagrangian velocities in open water. *J. Phys. Oceanogr.,* **13,** 1669–1680.

Dillon, T. M., J. G. Richman, C. G. Hansen, and M. D. Pearson, 1981: Near surface turbulence measurements in a lake. *Nature,* **290,** 390–392.

Dobroklonskiy, S. V., and B. M. Lesnikov, 1975: A laboratory study of the dynamic characteristics of drift currents in the presence of wind-driven waves. *Izv. Akad. Nauk. SSSR, Atmos. Ocean. Phys.,* **11,** 942–950.

Donelan, M., 1990: Air–sea interaction. *The Sea: Ocean Engineering Science,* Vol. 9, Part A, B. Le Mehaute and D. M. Hanes, Eds., Wiley and Sons, 239–292.

Efron, B., and G. Gong, 1983: A leisurely look at the bootstrap, the jacknife and cross-validation. *Amer. Statist.,* **37,** 36–48.

Forristall, G. Z., 1981: Measurements of a saturated range in the ocean wave spectra. *J. Geophys. Res.,* **86,** 8075–8084.

Gargett, A. E., 1989: Ocean turbulence. *Annu. Rev. Fluid Mech.,* **21,** 419–451.

Gregg, M. C., 1987: Structures and fluxes in a deep convecting mixed layer. *Dynamics of the Oceanic Mixed Layer,* P. Müller and D. Henderson, Eds., Hawaii Institute of Geophysics Special Publication, 1–23.

Hasselmann, K., T. P. Barnett, E. Bouws, H. Carlson, D. E. Cartwright, K. Enke, J. A. Ewing, H. Gienapp, D. E. Hasselmann, P. Krusemann, A. Meerburg, P. Müller, D. J. Olbers, K. Richter, W. Sell, and H. Walden, 1973: Measurements of wind-wave growth and swell decay during the Joint North Sea Wave Project (JONSWAP). *Dtsch. Hydrogr. Z.,* **A8**(Suppl.), 95 pp.

Haugen, D. A., J. C. Kaimal, and E. F. Bradley, 1971: An experimental study of Reynolds stress and heat flux in the atmospheric surface layer. *Quart. J. Roy. Meteor. Soc.,* **97,** 168–180.

Holthuijsen, L. H., and T. H. C. Herbers, 1986: Statistics of breaking waves observed as whitecaps in the open ocean. *J. Phys. Oceanogr.,* **16,** 290–297.

Holtslag, A. A. M., and F. T. M. Nieuwstadt, 1986: Scaling the atmospheric boundary layer. *Bound.-Layer Meteor.,* **36,** 201–209.

Huang, N. E., 1986: An estimate of the influence of breaking waves on the dynamics of the upper ocean. *Wave Dynamics and Radio Probing of the Ocean Surface,* O. M. Phillips and K. Hasselmann, Eds., Plenum, 295–313.

Hussain, A. K. M. F., and W. C. Reynolds, 1970: The mechanics of an organized wave in turbulent shear flow. Part 2: Experimental results. *J. Fluid Mech.,* **41,** 241–258.

Imberger, J., 1985: The diurnal mixed layer. *Limnol. Oceanogr.,* **30,** 737–770.

Jacobs, A. J., 1978: Numerical simulations of the natural variability in water temperature during BOMEX using alternative forms of the vertical eddy exchange coefficients. *J. Phys. Oceanogr.,* **8,** 119–141.

Jones, I. S. F., and B. C. Kenney, 1977: The scaling of velocity fluctuations in the surface mixed layer. *J. Geophys. Res.,* **82,** 1392–1396.

Kitaigorodskii, S. A., 1961: On the possibility of theoretical calculation of vertical temperature profile in upper layers of the sea. *Bull. Acad. Sci. USSR, Geophys. Ser.,* **3,** 313–318.

——, 1983: On the theory of the equilibrium range in the spectrum of wind-generated gravity waves. *J. Phys. Oceanogr.,* **13,** 816–827.

——, 1984: On the fluid dynamical theory of turbulent gas transfer across an air–sea interface in the presence of breaking wind-waves. *J. Phys. Oceanogr.,* **14,** 960–972.

——, and J. L. Lumley, 1983: Wave-turbulence interactions in the upper ocean. Part I: The energy balance of the interacting fields of surface wind waves and wind-induced three-dimensional turbulence. *J. Phys. Oceanogr.,* **13,** 1977–1987.

——, M. A. Donelan, J. L. Lumley, and E. A. Terray, 1983: Wave-turbulence interactions in the upper ocean. Part 2: Statistical characteristics of wave and turbulent components of the random velocity field in the marine surface layer. *J. Phys. Oceanogr.,* **13,** 1988–1999.

Lamarre, E., and W. K. Melville, 1991: Air entrainment and dissipation in breaking waves. *Nature,* **351,** 469–472.

Large, W. G., and S. Pond, 1981: Open ocean momentum flux measurements in moderate to strong winds. *J. Phys. Oceanogr.,* **11,** 324–336.

Lombardo, C. P., and M. C. Gregg, 1989: Similarity scaling of viscous and thermal dissipation in a convecting surface boundary layer. *J. Geophys. Res.,* **94,** 6273–6284.

Longuet-Higgins, M. S., 1969: On wave breaking and the equilibrium spectrum of wind-generated waves. *Proc. Roy. Soc. London,* **A310,** 151–159.

Moum, J. N., M. C. Gregg, R. C. Lien, and M. E. Carr, 1995: Comparison of ϵ from two microstructure profilers. *J. Atmos. Oceanic Technol.,* **12,** 346–366.

Nasmyth, P., 1970: Oceanic turbulence. Ph.D. thesis, University of British Colombia, Vancouver, 69 pp.

Neumann, G., and W. J. Pierson Jr., 1966: *Principles of Physical Oceanography.* Prentice Hall, 545 pp.

Nicholls, S., and C. J. Readings, 1979: Aircraft observations of the structure of the lower boundary layer over the ocean. *Quart. J. Roy. Meteor. Soc.,* **105,** 785–802.

Ninnis, R., 1984: The effects of spatial averaging on airfoil probe measurements of oceanic velocity microstructure. Ph.D. thesis, University of British Colombia, Vancouver, 109 pp.

Oakey, N. S., and J. A. Elliott, 1982: Dissipation within the surface mixed layer. *J. Phys. Oceanogr.,* **12,** 171–185.

Osborn, T., D. M. Farmer, S. Vagle, S. A. Thorpe, and M. Cure, 1992: Measurements of bubble plumes and turbulence from a submarine. *Atmos.-Ocean,* **30,** 419–440.

Phillips, O. M., 1961: A note on the turbulence generated by gravity waves. *J. Geophys. Res.,* **66,** 2889–2893.

——, 1977: *The Dynamics of the Upper Ocean.* Cambridge University Press, 336 pp.

Press, W. H., B. P. Flannery, S. A. Teukolsky, and W. T. Vetterling, 1986: *Numerical Recipes.* Cambridge University Press, 818 pp.

Rapp, R. J., and W. K. Melville, 1990: Laboratory measurements of deep-water breaking waves. *Philos. Trans. Roy. Soc. London, Ser. A,* **331,** 735–800.

Richman, J., and C. Garrett, 1977: The transfer of energy and momentum by the wind to the surface mixed layer. *J. Phys. Oceanogr.*, **7**, 876–881.

Shay, T. J., and M. C. Gregg, 1984: Turbulence in an oceanic convective layer. *Nature*, **310**, 282–285.

Shonting, D. H., 1964: A preliminary investigation of momentum flux in ocean waves. *Pure Appl. Geophys.*, **57**, 149–152.

——, 1967: Measurements of particle motions in ocean waves. *J. Mar. Res.*, **25**, 162–181.

——, 1968: Autospectra of observed particle motion in wind waves. *J. Mar. Res.*, **26**, 411–419.

——, 1970: Observations of Reynolds stresses in wind waves. *Pure Appl. Geophys.*, **81**, 202–210.

Soloviev, A. V., 1986: Dissipation of turbulent energy in the wind-generated wave layer of the ocean. *Izv. Akad. Nauk. SSSR, Atmos. Oceanic Phys.*, **22**, 286–292.

——, N. V. Vershinsky, and V. A. Bezverchnii, 1988: Small scale turbulence measurements in the thin surface layer of the ocean. *Deep-Sea Res.*, **35**, 1859–1874.

——, ——, and ——, 1989: Small scale turbulence measurements in the thin surface layer of the ocean (Corrigenda). *Deep-Sea Res.*, **36**, 1283–1284.

Stewart, R. W., and H. L. Grant, 1962: Determination of the rate of dissipation of turbulent energy near the sea surface in the presence of waves. *J. Geophys. Res.*, **67**, 3177–3180.

Stull, R. B., 1988: *An Introduction to Boundary Layer Meteorology.* Kluwer Academic Publishers, 666 pp.

Tennekes, H., and J. L. Lumley, 1972: *A First Course in Turbulence.* The MIT Press, 300 pp.

Thorpe, S. A., 1982: On the clouds of bubbles formed by breaking waves in deep water and their role in air–sea gas transfer. *Philos. Trans. Roy. Soc. London, Ser. A*, **304**, 155–210.

——, 1984: On the determination of K_v in the near surface ocean from acoustic measurements of bubbles. *J. Phys. Oceanogr.*, **14**, 855–863.

——, and P. N. Humphries, 1980: Bubbles and breaking waves. *Nature*, **283**, 463–465.

Wyngaard, J. C., 1973: On surface layer turbulence. *Workshop on Micrometeorology*, P. M. Haugen, Ed., Amer. Meteor. Soc., 101–149.

Yefimov, V. V., and G. N. Khristoforov, 1969: Some features of the velocity field in the layer of wind-driven swell. *Izv. Akad. Nauk. SSSR, Atmos. Ocean. Phys.*, **5**, 597–602.

——, and ——, 1971: Spectra and statistical relations between the velocity fluctuations in the upper layer of the sea and surface waves. *Izv. Akad. Nauk. SSSR, Atmos. Ocean. Phys.*, **7**, 841–851.